JOURNAL OF COMPUTATIONAL PHYSICS 72, 311–346 (1987)

Monte Carlo Solutions of a Joint PDF Equation for Turbulent Flows in General Orthogonal Coordinates

D. C. HAWORTH* AND S. B. POPE

Sibley School of Mechanical and Aerospace Engineering, Cornell University, Ithaca, New York 14853

Received July 28, 1986; revised January 22, 1987

The modeled transport equation for the joint probability density function (pdf) of the velocities and a single scalar composition in a turbulent flow is an integro-differential equation in up to seven independent variables and time. Because of its large dimensionality, this equation may be efficiently solved by a Monte Carlo method. An algorithm is developed that allows the pdf equation to be solved in a general orthogonal coordinate system. The method is based on a Lagrangian approach in which the behavior of fluid particles in a turbulent flow is modeled and particle trajectories are computed in the Monte Carlo solution algorithm. The technique is applied to three self-similar turbulent free shear flows: the plane mixing layer, the plane jet, and the axisymmetric jet. Numerical test results are presented which compare the new algorithm with earlier methods, verify the statistical error estimates, and demonstrate convergence.

I. INTRODUCTION

A numerical algorithm is developed for the solution (in general orthogonal coordinates) of a joint probability density function (pdf) transport equation that arises in the study of turbulent fluid flow. The pdf considered is the one-point joint probability density function of the Eulerian velocities and scalars, the "velocity-composition" joint pdf. The method of modeling and solving a transport equation for a pdf as an approach to turbulence closures originated with the work of Lundgren [1, 2] and has subsequently been refined and developed by several investigators [3–5]. Recent papers by Pope and coworkers [6–13] contain modeling studies based on the solution of a modeled velocity–composition joint pdf equation. These calculations demonstrate the strength of the pdf approach in the treatment of complex turbulent flows including those with variable density and reaction. A comprehensive account of the pdf method for turbulent flows including the Monte Carlo method is provided by Pope [14].

At first sight, the pdf method seems to be of little more than academic interest due to the apparent difficulty in obtaining solutions to the resulting modeled

* Present address: Fluid Mechanics Department, General Motors Research Laboratories, Warren, Michigan 48090.

0021-9991/87 $3.00

equations. Even in constant-property inert flows, the modeled velocity–composition joint pdf transport equation (for a single scalar) is an integro-differential equation in up to seven independent variables and time. In flows of practical interest, analytic solutions are out of the question, and conventional numerical techniques (e.g., finite-difference methods) are impracticable. However, it is possible to solve the modeled pdf equation by a Monte Carlo method, a numerical method that is ideally suited to problems of large dimensionality [15, 16]. In the Monte Carlo method, computational requirements increase only linearly with the dimensionality of the pdf, while for finite-difference methods, it can be estimated that the increase is exponential [17]. This technique was originally proposed and developed by Pope [17, 14], and its feasibility has been amply demonstrated [6–13]. But no demonstration of convergence of the numerical method has been presented. Monte Carlo algorithms have been used for statistically one-dimensional time-dependent flows [8, 9, 11, 13] and for statistically two-dimensional boundary-layer type flows [10, 12], both in Cartesian coordinates. In fact, the flows studied by Pope and Correa [12] and by Pope and Cheng [13] are in cylindrical and spherical coordinates, respectively, but were solved using a pseudo-Cartesian algorithm. This is discussed further at the end of Section IV.

It is desirable to extend the method to non-Cartesian coordinates. Non-Cartesian coordinate systems are convenient in two situations. The most obvious case is a flow where boundary conditions or some other physical feature (e.g., body forces) are most naturally described in a non-Cartesian frame. The second case is more subtle. While the Monte Carlo method is well suited to a large number of dimensions, there is a computational advantage in minimizing the dimensionality in physical space. This dimensionality can sometimes be reduced by introducing a transformed coordinate system. It is the latter situation that is of primary interest in this paper. The self-similar axisymmetric jet, for example, is statistically three-dimensional in Cartesian coordinates, but by a suitable transformation to non-Cartesian coordinates, it can be rendered one-dimensional. This flow and two other examples are treated in Section IV.

Another motivation for the development of the new algorithm is that the current boundary-layer method is restricted to flows where the streamwise mean velocity is nowhere very small compared to a characteristic velocity difference (see Section V); it cannot be applied to self-similar jets in stagnant surroundings or to low velocity ratio mixing layers ($U_L/U_H \to 0$, Fig. 1), flows which are of both practical and theoretical interest in the study of turbulence. The computational method used (but not explained in detail) by Pope [6, 7] for the self-similar plane jet is similar to the technique developed here: the present approach is both a generalization and an improvement of the earlier method.

The contributions of this paper towards the development of solution algorithms for the pdf transport equation are as follows. First, a general algorithm is developed that allows the modeled pdf transport equation to be solved in non-Cartesian orthogonal coordinate systems. Second, the new method is applied to three self-similar turbulent flows of practical interest: the plane mixing layer, the plane jet,

and the axisymmetric jet. Third, for one flow (the plane mixing layer) it is demonstrated that three different solution algorithms, including the new one developed here, agree in appropriate limiting cases. And fourth, numerical tests are presented that demonstrate convergence of the Monte Carlo method.

The algorithm developed is independent of the specific models chosen: fairly crude models are used here for simplicity. While we focus on a pdf equation that is derived from the equations governing turbulent fluid flow, the material concerning coordinate system transformations and the discrete representation may be applicable to pdf equations or other tensor density equations that arise in different fields of study.

We begin in Section II with an overview of the pdf method including basic definitions, modeling, and a solution algorithm for Cartesian coordinate systems. In Section III, transformation rules to general orthogonal coordinate systems are presented and a Monte Carlo method appropriate to these coordinates is introduced. This material is difficult and somewhat involved because of the nature of the quantities being transformed: we are working with tensor densities, not functions. Specific forms for the three self-similar flows mentioned earlier are given in Section IV. Section V contains the computational results. A comparison is made among three solution algorithms for the self-similar plane mixing layer; conclusions are then drawn concerning the limitations of these algorithms. The statistical error inherent in the Monte Carlo method is investigated and convergence is demonstrated. Finally, a summary and conclusions are given in Section VI.

II. Background

This section contains a summary of those features of the pdf method, the modeling, and the Monte Carlo solution technique that are needed in the development of the new numerical algorithm. These are presented in a form appropriate to Cartesian coordinate systems. For concreteness, specific models are selected for analysis, but the algorithms to be developed in Sections III and IV are not limited to these models. Further details on the material in this section can be found in Ref. [14].

II.1. *Pdf Method*

We begin by considering the turbulent flow of a variable density fluid, including chemical reaction. The Eulerian velocity, scalar ("composition"), and pressure fields are denoted by $\mathbf{U}(\mathbf{x}, t)$, $\Phi(\mathbf{x}, t)$, and $p(\mathbf{x}, t)$, respectively. The body force per unit mass is g and the rate of increase of Φ due to reaction is S. The fluid density is denoted by ρ; τ_{ij} is the viscous stress tensor and $\mathbf{J}$ is the diffusive mass flux vector of Φ. We limit our attention to flows where the fluid properties and S are unique functions of the single scalar Φ [14]; all information about the flow field is then contained in the Eulerian conservation equations for mass, momentum, and the

scalar. In Cartesian tensor notation with the usual summation convention on repeated indices, these equations are

$$\frac{\partial \rho}{\partial t} + \frac{\partial (\rho U_i)}{\partial x_i} = 0, \tag{1}$$

$$\frac{\partial U_i}{\partial t} + U_j \frac{\partial U_i}{\partial x_j} = \frac{1}{\rho}\frac{\partial \tau_{ij}}{\partial x_j} - \frac{1}{\rho}\frac{\partial p}{\partial x_i} + g_i, \tag{2}$$

$$\frac{\partial \Phi}{\partial t} + U_i \frac{\partial \Phi}{\partial x_i} = -\frac{1}{\rho}\frac{\partial J_i}{\partial x_i} + S. \tag{3}$$

Additional scalars may be included simply by making Φ be a vector-valued quantity. Then $\rho = \rho(\boldsymbol{\Phi})$, $\mathbf{S} = \mathbf{S}(\boldsymbol{\Phi})$, etc.

Due to the difficulty in obtaining full solutions of these equations in a turbulent flow, and because it is generally only mean quantities that are of interest, a statistical approach is usually adopted [14, 18]. The approach of interest here is the pdf method. The goal of the pdf method is to determine the evolution of the velocity–composition joint pdf $f(\mathbf{V}, \Psi; \mathbf{x}, t)$. This is the joint probability density of the event $\{\mathbf{U}(\mathbf{x}, t) = \mathbf{V}, \Phi(\mathbf{x}, t) = \Psi\}$. Knowing the one-point joint pdf is equivalent to knowing all one-point statistics of the Eulerian velocity and scalar fields. This pdf is a tensor density in the 4-dimensional velocity–composition space; it is also a function of position and of time. The pdf is defined such that when multiplied by an infinitesimal volume element in the velocity–composition space (denoted by $d\mathbf{V}\, d\Psi$) the result is the probability that the Eulerian velocities and scalar at position $\mathbf{x}$ and time t lie inside this element:

$$f(\mathbf{V}, \Psi; \mathbf{x}, t)\, d\mathbf{V}\, d\Psi = \text{Prob}\{V_i < U_i(\mathbf{x}, t) \leqslant V_i + dV_i,\ i = 1, 2, 3;\ \Psi < \Phi(\mathbf{x}, t) \leqslant \Psi + d\Psi\}. \tag{4}$$

The properties of the pdf follow from this definition: it is nonnegative since it represents a probability

$$f(\mathbf{V}, \Psi; \mathbf{x}, t) \geqslant 0; \tag{5}$$

over the entire 4-dimensional velocity–composition space it integrates to unity

$$\iint f(\mathbf{V}, \Psi; \mathbf{x}, t)\, d\mathbf{V}\, d\Psi = 1; \tag{6}$$

and, most importantly, the mean of any function of the velocities and scalars $Q[\mathbf{U}(\mathbf{x}, t), \Phi(\mathbf{x}, t)]$ can be expressed as an integral over the pdf, or as a probability weighted integral

$$\iint Q(\mathbf{V}, \Psi) f(\mathbf{V}, \Psi; \mathbf{x}, t)\, d\mathbf{V}\, d\Psi = \langle Q(\mathbf{x}, t) \rangle. \tag{7}$$

Angled brackets $\langle\ \rangle$ are used to denote means throughout this paper.

In variable-density flows, it is convenient to work with density-weighted means, or Favre averages [19]. The density-weighted mean $\tilde{Q}$ of a random variable $Q(\mathbf{U}, \Phi)$ is defined by

$$\tilde{Q} \equiv \langle \rho Q \rangle / \langle \rho \rangle, \tag{8}$$

and the fluctuation about this mean is

$$Q'' \equiv Q - \tilde{Q}. \tag{9}$$

We then decompose the Eulerian velocity and scalar fields into their (Favre-averaged) mean components $\tilde{\mathbf{U}}(\mathbf{x}, t)$, $\tilde{\Phi}(\mathbf{x}, t)$ and their Favre fluctuations $\mathbf{u}''(\mathbf{x}, t)$, $\Phi''(\mathbf{x}, t)$,

$$\mathbf{U}(\mathbf{x}, t) = \tilde{\mathbf{U}}(\mathbf{x}, t) + \mathbf{u}''(\mathbf{x}, t), \tag{10}$$

$$\Phi(\mathbf{x}, t) = \tilde{\Phi}(\mathbf{x}, t) + \Phi''(\mathbf{x}, t), \tag{11}$$

while conventional averaging is used for the pressure field,

$$p(\mathbf{x}, t) = \langle p(\mathbf{x}, t) \rangle + p'(\mathbf{x}, t). \tag{12}$$

The density-weighted joint pdf $\tilde{f}(\mathbf{V}, \Psi; \mathbf{x}, t)$ is defined by

$$\tilde{f}(\mathbf{V}, \Psi; \mathbf{x}, t) \equiv f(\mathbf{V}, \Psi; \mathbf{x}, t)\, \rho(\Psi) / \langle \rho(\mathbf{x}, t) \rangle, \tag{13}$$

where $\tilde{f}$ has the properties of a pdf, Eqs. (5) and (6). In terms of $\tilde{f}$, density-weighted means are expressed as

$$\iint Q(\mathbf{V}, \Psi) \tilde{f}(\mathbf{V}, \Psi; \mathbf{x}, t)\, d\mathbf{V}\, d\Psi = \tilde{Q}(\mathbf{x}, t), \tag{14}$$

analogous to Eq. (7). Note that in a uniform-density flow, $\tilde{Q} = \langle Q \rangle$ and $\tilde{f} = f$.

A third density function that is useful in the description of variable-density turbulent flows is the mass density function (mdf) F,

$$F(\mathbf{V}, \Psi, \mathbf{x}; t) \equiv \rho(\Psi) f(\mathbf{V}, \Psi; \mathbf{x}, t) = \langle \rho(\mathbf{x}, t) \rangle \tilde{f}(\mathbf{V}, \Psi; \mathbf{x}, t). \tag{15}$$

The properties of F follow from this definition and from the properties of f and $\tilde{f}$:

$$\iint F(\mathbf{V}, \Psi, \mathbf{x}; t)\, d\mathbf{V}\, d\Psi = \langle \rho \rangle, \tag{16}$$

$$\iint F(\mathbf{V}, \Psi, \mathbf{x}; t)\, [\rho(\Psi)]^{-1}\, d\mathbf{V}\, d\Psi = 1, \tag{17}$$

$$\iint F(\mathbf{V}, \Psi, \mathbf{x}; t)\, Q(\mathbf{V}, \Psi)\, d\mathbf{V}\, d\Psi = \langle \rho Q \rangle = \langle \rho \rangle \tilde{Q}. \tag{18}$$

In these equations, the means are functions of $\mathbf{x}$ and of t. The mdf is a density with respect to $\mathbf{x}$ as well as with respect to $\mathbf{V}$ and Ψ. Equation (15) is valid only in a Cartesian coordinate system; the generalization to non-Cartesian systems is discussed in Section III.

The evolution equation for F is derived from Eqs. (1)–(3) [5, 14],

$$\frac{\partial F}{\partial t} + V_i \frac{\partial F}{\partial x_i} + \left(g_i - \frac{1}{\rho(\Psi)} \frac{\partial \langle p \rangle}{\partial x_i} \right) \frac{\partial F}{\partial V_i} + \frac{\partial}{\partial \Psi} [F S(\Psi)]$$
$$= -\frac{\partial}{\partial V_i} \left[\frac{F}{\rho(\Psi)} \left\langle \frac{\partial \tau_{ij}}{\partial x_j} - \frac{\partial p'}{\partial x_i} \,|\, \mathbf{U}(\mathbf{x}, t) = \mathbf{V}, \Phi(\mathbf{x}, t) = \Psi \right\rangle \right]$$
$$+ \frac{\partial}{\partial \Psi} \left[\frac{F}{\rho(\Psi)} \left\langle \frac{\partial J_i}{\partial x_i} \,|\, \mathbf{U}(\mathbf{x}, t) = \mathbf{V}, \Phi(\mathbf{x}, t) = \Psi \right\rangle \right]. \tag{19}$$

The mean pressure field can be expressed in terms of one-point statistics of the velocity field using a Poisson equation for the mean pressure, so that no modeling is required for the left-hand side of Eq. (19). The notation $\langle A \,|\, B \rangle$ denotes the conditional expectation of the event A, given event B; thus in Eq. (19), $\langle \partial \tau_{ij}/\partial x_i \,|\, \mathbf{U}(\mathbf{x}, t) = \mathbf{V}, \Phi(\mathbf{x}, t) = \Psi \rangle$ is the mean of $\partial \tau_{ij}/\partial x_i$ conditional of the event $\{\mathbf{U}(\mathbf{x}, t) = \mathbf{V}, \Phi(\mathbf{x}, t) = \Psi\}$, and similarly for the other terms on the right-hand side. These conditional expectations cannot be expressed in terms of the one-point pdf, and hence must be modeled.

II.2. *Modeling*

In the pdf method, it is most convenient both for the modeling and for the solution algorithm to adopt a Lagrangian approach; modeling the behavior of fluid particles in a turbulent flow provides closure models for the conditional expectations on the right-hand side of Eq. (19). Let $\mathbf{x}^+(t)$, $\mathbf{U}^+(t)$, and $\Phi^+(t)$ denote the position, velocity, and composition of a fluid particle at time t. The relationship between Lagrangian quantities and the corresponding Eulerian fields is given by

$$\mathbf{U}^+(t) = \mathbf{U}[\mathbf{x}^+(t), t], \qquad \Phi^+(t) = \Phi[\mathbf{x}^+(t), t]. \tag{20}$$

That is, the velocity and composition of a fluid particle is equal to the value of the corresponding Eulerian field at the position occupied by the particle. The rate of change of position of a fluid particle is its velocity, the velocity of a particle changes in accordance with the Navier–Stokes equation (Eq. (2)) and the particle composition changes by Eq. (3):

$$dx_i^+ = U_i^+ \, dt, \tag{21}$$

$$dU_i^+ = \left(g_i - \frac{1}{\rho(\Phi^+)} \frac{\partial \langle p \rangle}{\partial x_i} \right) dt + \left(\frac{1}{\rho(\Phi^+)} \frac{\partial \tau_{ij}}{\partial x_j} - \frac{1}{\rho(\Phi^+)} \frac{\partial p'}{\partial x_i} \right) dt, \tag{22}$$

$$d\Phi^+ = S(\Phi^+) \, dt - \frac{1}{\rho(\Phi^+)} \frac{\partial J_i}{\partial x_i} \, dt, \tag{23}$$

where the Eulerian variables on the right-hand sides are evaluated at the particle position $\mathbf{x}^+(t)$.

In the pdf method, the fluctuating pressure gradient and viscous terms in Eq. (22) and the molecular diffusivity term on the right-hand side of Eq. (23) are modeled, usually by stochastic processes. Using a superscript * to indicate a property of a modeled particle, we can write

$$dx_i^* = U_i^*\, dt, \tag{24}$$

$$dU_i^* = A_i^*\, dt, \tag{25}$$

$$d\Phi^* = B^*\, dt, \tag{26}$$

where $A_i^*\, dt$ and $B^*\, dt$ model the right-hand sides of Eqs. (22) and (23), respectively.

One set of models that has been suggested for the particle velocity corresponds to a stochastic diffusion process for the effects of the viscosity and the fluctuating pressure gradient terms in Eq. (22) [20]. In the simplest diffusion model, the particle velocities are governed by a stochastic differential equation of the Langevin type [8],

$$dU_i^* = \left(g_i - \frac{1}{\rho(\Phi^*)}\frac{\partial\langle p\rangle}{\partial x_i}\right)dt - \left(\frac{1}{2}+\frac{3}{4}C_0\right)(U_i^* - \tilde{U}_i)\frac{dt}{\tau} + (C_0\varepsilon)^{1/2}\, dW_i(t). \tag{27}$$

In this equation, $\varepsilon(\mathbf{x}, t)$ is the viscous dissipation rate of the turbulent kinetic energy k, where

$$k \equiv \frac{\langle \rho u_i'' u_i''\rangle}{2\langle\rho\rangle}. \tag{28}$$

A characteristic time scale of the turbulence is $\tau(\mathbf{x}, t)$ defined by

$$\tau \equiv k/\varepsilon. \tag{29}$$

The model constant C_0 is ascribed the value 2.1 [8]. The isotropic Wiener process $\mathbf{W}(t)$ is a continuous Markovian stochastic process whose increments $d\mathbf{W}(t)$ have a joint-normal distribution with zero means and an isotropic covariance matrix,

$$\langle dW_i(t)\rangle = 0, \qquad \langle dW_i(t)\, dW_j(t)\rangle = dt\, \delta_{ij}, \tag{30}$$

where δ_{ij} denotes the Kronecker delta. Further information concerning this Langevin model and its applications in turbulent flows is contained in Refs. [8, 11, 14, 21].

For the molecular diffusivity, we take the simple linear deterministic model proposed by Dopazo [22],

$$d\Phi^* = S(\Phi^*)\, dt - \frac{1}{2}C_\Phi(\Phi^* - \tilde{\Phi})\frac{dt}{\tau}, \tag{31}$$

where C_Φ is a model constant, with $C_\Phi = 2.0$ being the usual value [14]. It should be realized that this model is physically unrealistic (see Ref. [14], for example) and its use here is solely illustrative.

The modeled pdf equation corresponding to Eqs. (24), (27), and (31) is

$$\frac{\partial F}{\partial t} + V_i \frac{\partial F}{\partial x_i} + \left(g_i - \frac{1}{\rho(\Psi)} \frac{\partial \langle p \rangle}{\partial x_i} \right) \frac{\partial F}{\partial V_i} + \frac{\partial}{\partial \Psi} [F S(\Psi)]$$

$$= \left(\frac{1}{2} + \frac{3}{4} C_0 \right) \frac{1}{\tau} \frac{\partial}{\partial V_i} [F(V_i - \tilde{U}_i)] + \frac{1}{2} C_0 \varepsilon \frac{\partial^2 F}{\partial V_i \partial V_i}$$

$$+ \frac{C_\Phi}{2\tau} \frac{\partial}{\partial \Psi} [F(\Psi - \tilde{\Phi})]. \tag{32}$$

For this equation to be closed, an additional model is needed for the dissipation rate ε or for the turbulent time scale τ: ε may be obtained from a modeled equation [18] or τ may be specified directly [7]. Henceforth, ε and τ are assumed to be known. Recalling that $\langle p \rangle$ and k can be expressed as integrals over the pdf, it may be seen that Eq. (32) is an integro-differential equation in up to seven independent variables and time.

II.3. *Monte Carlo Method*

The modeled pdf evolution equation (Eq. (32)) has been derived from modeled particle equations (Eqs. (24), (27), and (31)). It is reasonable, then, to base a Monte Carlo solution method for Eq. (32) on the numerical solution of these particle equations for a large number of particles N. Each of the particles exists in a 7-dimensional velocity–composition–position state space. The particle positions, velocities, and compositions evolve according to the modeled Lagrangian equations, which must be written in discretized form for numerical implementation. A finite difference approximation of the ordinary differential equation (Eq. (31)) is obtained in a straightforward manner; derivation of difference approximations for the stochastic ordinary differential equations (Eqs.(24) and (27)) requires some knowledge of stochastic calculus [23]. A discretization that is first order in the computational time step h is

$$\Delta x_i^* \equiv x_i^*(t+h) - x_i^*(t) = U_i^* h, \tag{33}$$

$$\Delta U_i^* \equiv U_i^*(t+h) - U_i^*(t)$$

$$= \left(g_i - \frac{1}{\rho(\Phi^*)} \frac{\partial \langle p \rangle}{\partial x_i} \right) h - \left(\frac{1}{2} + \frac{3}{4} C_0 \right) (U_i^* - \tilde{U}_i) \frac{h}{\tau} + (C_0 \varepsilon h)^{1/2} \xi_i, \tag{34}$$

$$\Delta \Phi^* \equiv \Phi^*(t+h) - \Phi^*(t) = S(\Phi^*)\, h - \frac{1}{2} C_\Phi (\Phi^* - \tilde{\Phi}) \frac{h}{\tau}, \tag{35}$$

where all quantities on the right-hand sides are evaluated at time level t. Hence ξ is a vector of independent standardized Gaussian random variables:

$$\langle \xi_i \rangle = 0, \qquad \langle \xi_i \xi_j \rangle = \delta_{ij}. \tag{36}$$

Equation (34) is a Gaussian random walk in velocity space. Higher order numerical schemes have also been developed [23].

The precise relationship between particle properties $\{\mathbf{x}^*, \mathbf{U}^*, \Phi^*\}$ and the pdf $\tilde{f}$ is less obvious. To elucidate this connection, we introduce a discretization of the mass density function (mdf). Within the volume in physical space V, the mdf is represented by N particles, each representing a mass of fluid Δm. The nth particle—the numbering being arbitrary—has position $\mathbf{x}^{(n)}$, velocity $\mathbf{U}^{(n)}$, and composition $\Phi^{(n)}$. The discrete mass density function $F^*(\mathbf{V}, \Psi, \mathbf{x}; t)$ is defined by

$$F^*(\mathbf{V}, \Psi, \mathbf{x}; t) \equiv \Delta m \sum_{n=1}^{N} \delta(\mathbf{V} - \mathbf{U}^{(n)}(t))\, \delta(\Psi - \Phi^{(n)}(t))\, \delta(\mathbf{x} - \mathbf{x}^{(n)}(t)). \tag{37}$$

Here, $\delta(\mathbf{x} - \mathbf{x}^{(n)}(t))$ is a 3-dimensional delta function

$$\delta(\mathbf{x} - \mathbf{x}^{(n)}(t)) \equiv \delta(x_1 - x_1^{(n)}(t))\, \delta(x_2 - x_2^{(n)}(t))\, \delta(x_3 - x_3^{(n)}(t)), \tag{38}$$

and similarly for $\delta(\mathbf{V} - \mathbf{U}^{(n)}(t))$. Denoting by M the total mass in the volume V ($M = N \cdot \Delta m$), the expectation of Eq. (37) is

$$\langle F^*(\mathbf{V}, \Psi, \mathbf{x}; t) \rangle = M \langle \delta(\mathbf{V} - \mathbf{U}^*(t))\, \delta(\Psi - \Phi^*(t))\, \delta(\mathbf{x} - \mathbf{x}^*(t)) \rangle, \tag{39}$$

where the * refers to any particle n, $1 \leqslant n \leqslant N$.

The particle properties are deduced by requiring that this discrete representation be a consistent representation of the mdf in the mean, i.e.,

$$\langle F^*(\mathbf{V}, \Psi, \mathbf{x}; t) \rangle = F(\mathbf{V}, \Psi, \mathbf{x}; t). \tag{40}$$

We let $l(\mathbf{x})$ be the pdf of particle positions, that is, the pdf of the event $\mathbf{x}^* = \mathbf{x}$,

$$l(\mathbf{x}) \equiv \langle \delta(\mathbf{x} - \mathbf{x}^*(t)) \rangle. \tag{41}$$

Integrating Eq. (39) over velocity–composition space yields

$$\iint \langle F^* \rangle \, d\mathbf{V}\, d\Psi = M \langle \delta(\mathbf{x} - \mathbf{x}^*(t)) \rangle = M l(\mathbf{x}), \tag{42}$$

while integrating Eq. (40) gives (see Eq. 16)

$$\iint \langle F^* \rangle \, d\mathbf{V}\, d\Psi = \langle \rho(\mathbf{x}, t) \rangle. \tag{43}$$

Thus, a necessary condition for Eq. (40) to hold is

$$l(\mathbf{x}) = \langle \rho(\mathbf{x}, t) \rangle / M: \tag{44}$$

the density of particles in physical space is proportional to the mean fluid density. The pdf of particle properties at a fixed location $\mathbf{x}^* = \mathbf{x}$ is $f^*(\mathbf{V}, \Psi; t \mid \mathbf{x}^* = \mathbf{x})$, where

$$f^*(\mathbf{V}, \Psi; t \mid \mathbf{x}^* = \mathbf{x}) \equiv \frac{\langle \delta(\mathbf{V} - \mathbf{U}^*(t))\, \delta(\Psi - \Phi^*(t))\, \delta(\mathbf{x} - \mathbf{x}^*(t)) \rangle}{\langle \delta(\mathbf{x} - \mathbf{x}^*(t)) \rangle}. \tag{45}$$

Using Eqs. (15), (39)–(41), (44), and (45), it may be seen that

$$f^*(\mathbf{V}, \Psi; t \mid \mathbf{x}^* = \mathbf{x}) = \frac{F}{M} \frac{1}{l(\mathbf{x})} = \frac{F}{M} \frac{M}{\langle \rho \rangle} = \frac{F}{\langle \rho \rangle} = \tilde{f}(\mathbf{V}, \Psi; \mathbf{x}, t): \tag{46}$$

the distribution function of particle velocities and compositions at a given location is the density-weighted velocity–composition joint pdf.

The validity of the Monte Carlo method rests on the consistency between the discrete representation of the mdf and the exact mdf, Eq. (40): given the same initial and boundary conditions, $\langle F^* \rangle$ and F evolve in the same way for all time [14]. It can be shown that a necessary and sufficient condition for F (or $\langle F^* \rangle$) to remain a valid mdf for all time (i.e., to satisfy the realizability condition of Eq. (5), the consistency condition of Eq. (16), and the normalization condition of Eq. (17)) given that it is a valid mdf initially, is the satisfaction of the mean continuity equation. The mean continuity equation is simply the mean of Eq. (1):

$$\frac{\partial \langle \rho \rangle}{\partial t} + \frac{\partial \langle \rho U_i \rangle}{\partial x_i} = \frac{\partial \langle \rho \rangle}{\partial t} + \frac{\partial [\langle \rho \rangle \tilde{U}_i]}{\partial x_i} = 0. \tag{47}$$

This equation also follows on integration of the mdf evolution equation (Eqs. (19) or (32)) over all velocity and composition space. Equation (47) is satisfied provided that the mean pressure $\langle p \rangle$ evolves according to a Poisson equation [14].

The extraction of density-weighted means $\tilde{Q}$ from the discrete representation is discussed later. For the homogeneous case (in which $\tilde{f}$ independent of $\mathbf{x}$), it suffices simply to take the mass-weighted ensemble average over the N particles,

$$\tilde{Q} \approx \tilde{Q}_N = \frac{1}{N} \sum_{n=1}^{N} \Delta m\, Q(\mathbf{U}^{(n)}, \Phi^{(n)}) \Big/ \frac{1}{N} \sum_{n=1}^{N} \Delta m. \tag{48}$$

The ensemble average $\tilde{Q}_N$ is itself a random variable. According to Eqs. (24), (27), and (31), each particle evolves independently. Simple statistical analysis then shows that, as N tends, to infinity, the distribution of $\tilde{Q}_N$ approaches a normal distribution with mean

$$E_Q \equiv \langle \tilde{Q}_N \rangle = \tilde{Q}, \tag{49}$$

and variance

$$\sigma^2 \equiv \langle (\tilde{Q}_N - \tilde{Q})^2 \rangle = \frac{1}{N} \langle (Q - \tilde{Q})^2 \rangle. \tag{50}$$

The standard deviation σ is a measure of the statistical error in approximating means as ensemble avarages over particles.

To summarize: the Lagrangian solution algorithm outlined above is a Monte Carlo solution method for the modeled pdf evolution equation, Eq. (32). Each particle represents a fixed mass of fluid and can be viewed as an independent realization of the flow or as a delta function discretization of the mdf. The particle number density in physical space is proportional to the mean fluid density and the distribution of particles in velocity–composition space at a fixed position $\mathbf{x}$ is the density-weighted pdf. In the limit as $N \to \infty$ and as $h \to 0$, the solution converges to an exact solution of the modeled pdf transport equation. These notions are made rigorous in Ref. [14]. The chief merit of the Monte Carlo method is that it replaces the single partial differential equation for the joint pdf by $7N$ (stochastic) ordinary differential equations for the particles. This is a considerable simplification numerically. The computational requirements increase only linearly with the dimensionality of the pdf in the Monte Carlo method, while for finite-difference methods, this increase is exponential [17]. The main disadvantage of Monte Carlo methods is the slow convergence of the statistical error as $N^{-1/2}$ (Eq. (50)).

III. Non-Cartesian Coordinate Systems

In this section, the Lagrangian description and Monte Carlo solution algorithm of Section II are adapted to allow solution of the modeled pdf equation in non-Cartesian coordinate systems. The goal is to devise a discrete representation that is consistent with the modeled pdf transport equation in the new coordinate system. The transformation from Cartesian to general orthogonal coordinates is treated first. This is followed by the development of the discrete representation and the Monte Carlo solution algorithm.

III.1. *Coordinate System Transformations*

Consider the transformation from Cartesian coordinates $\mathbf{x} = \{x_1, x_2, x_3\}$ to the general orthogonal coordinates $\bar{\mathbf{x}} = \{\bar{x}_1, \bar{x}_2, \bar{x}_3\}$. Let $\{\mathbf{e}_1, \mathbf{e}_2, \mathbf{e}_3\}$ denote a set of orthonormal basis vectors in the $\{x_1, x_2, x_3\}$ directions, respectively, and $\{\bar{\mathbf{e}}_1, \bar{\mathbf{e}}_2, \bar{\mathbf{e}}_3\}$ denote a set of orthonormal basis vectors in the $\{\bar{x}_1, \bar{x}_2, \bar{x}_3\}$ directions. The change in the position vector $\mathbf{r}$ corresponding to increments in $\{\bar{x}_1, \bar{x}_2, \bar{x}_3\}$ defines the scale factors $h_{(i)}$ by the relationship

$$d\mathbf{r} = dx_i\, \mathbf{e}_i = h_{(i)}\, d\bar{x}_i\, \bar{\mathbf{e}}_i. \tag{51}$$

Even though we are no longer dealing (exclusively) with Cartesian tensors, we

retain the summation convention on all but bracketed suffices. Hence the final term in Eq. (51) is to be interpreted as

$$h_{(i)}\, d\bar{x}_i\, \bar{\mathbf{e}}_i = h_1\, d\bar{x}_1\, \bar{\mathbf{e}}_1 + h_2\, d\bar{x}_2\, \bar{\mathbf{e}}_2 + h_3\, d\bar{x}_3\, \bar{\mathbf{e}}_3. \tag{52}$$

The physical components of a vector $\mathbf{P}$ in the two systems are denoted by P_i and $\bar{P}_i$, respectively:

$$\mathbf{P} = P_i \mathbf{e}_i = \bar{P}_i \bar{\mathbf{e}}_i. \tag{53}$$

These components obey the transformation rule

$$\bar{P}_i = a_{ij} P_j, \tag{54}$$

where a_{ij} are the direction cosines $a_{ij} = \bar{\mathbf{e}}_i \cdot \mathbf{e}_j$. It is convenient to introduce a scaled velocity vector in the transformed coordinate system. The components of this scaled velocity are related to the physical velocity components via a stretching factor $\mu(\bar{\mathbf{x}})$. Thus the transformed velocity components $\bar{U}_i$ are

$$\bar{U}_i = \mu(\bar{\mathbf{x}})\, a_{ij} U_j. \tag{55}$$

These are equal to the physical velocity components only if $\mu(\bar{\mathbf{x}}) \equiv 1$. The scalar transforms trivially under this set of transformations,

$$\bar{\Phi} = \Phi. \tag{56}$$

A dot over a quantity is used to indicate the material derivative or the time rate of change following a particle. The material derivative of the position coordinates is given by

$$\dot{\bar{x}}_i = \frac{\bar{U}_i}{\mu h_{(i)}}, \tag{57}$$

and that of the velocity components by

$$\dot{\bar{U}}_i = \mu a_{ij} \dot{U}_j + C_i, \tag{58}$$

where

$$C_i = (\dot{\mu a_{ij}})\, U_j = U_j U_l \frac{\partial(\mu a_{ij})}{\partial x_l} = \frac{\bar{U}_k \bar{U}_p}{\mu^2} \frac{a_{kj}}{h_{(p)}} \frac{\partial(\mu a_{ij})}{\partial \bar{x}_p}. \tag{59}$$

The Jacobian of the transformation in physical space is denoted by J_x,

$$J_x \equiv \left| \frac{\partial(\bar{\mathbf{x}})}{\partial(\mathbf{x})} \right| = \frac{1}{h_1 h_2 h_3}, \tag{60}$$

and that of the velocity space transformation by J_U,

$$J_U \equiv \left| \frac{\partial(\bar{\mathbf{U}})}{\partial(\mathbf{U})} \right| = \mu^3. \tag{61}$$

For the transformation between the two seven-dimensional velocity–composition–position state spaces, the Jacobian J is

$$J \equiv \left| \frac{\partial(\bar{\mathbf{x}}, \bar{\mathbf{U}}, \bar{\Phi})}{\partial(\mathbf{x}, \mathbf{U}, \Phi)} \right| = J_x J_U = \frac{\mu^3}{h_1 h_2 h_3}. \tag{62}$$

The analysis is restricted to those transformations for which the Jacobians of Eqs. (60)–(62) are strictly positive.

The density functions $F(\mathbf{V}, \Psi, \mathbf{x}; t)$, $\tilde{f}(\mathbf{V}, \Psi; \mathbf{x}, t)$, and $f(\mathbf{V}, \Psi; \mathbf{x}, t)$ are tensor densities that transforme by the Jacobians of the transformations of their respective sample spaces. (By convention, the sample space variables appear to the left of the semicolons.) Velocity and composition sample space variables transform by Eqs. (55) and (56), $\bar{V}_i = \mu a_{ij} V_j$ and $\bar{\Psi} = \Psi$. Using an overbar to denote these density functions in the transformed coordinate system, the transformed mdf $\bar{F}(\bar{\mathbf{V}}, \bar{\Psi}, \bar{\mathbf{x}}; t)$ is related to $F(\mathbf{V}, \Psi, \mathbf{x}; t)$ by

$$J\bar{F}(\bar{\mathbf{V}}, \bar{\Psi}, \bar{\mathbf{x}}; t) = F(\mathbf{V}, \Psi, \mathbf{x}; t), \tag{63}$$

and the transformed density-weighted joint pdf $\bar{\tilde{f}}(\bar{\mathbf{V}}, \bar{\Psi}; \bar{\mathbf{x}}, t)$ is related to $\tilde{f}(\mathbf{V}, \Psi; \mathbf{x}, t)$ by

$$J_U \bar{\tilde{f}}(\bar{\mathbf{V}}, \bar{\Psi}; \bar{\mathbf{x}}, t) = \tilde{f}(\mathbf{V}, \Psi; \mathbf{x}, t). \tag{64}$$

Combining Eqs. (15) and (62)–(64), we obtain the relationship between $\bar{F}$ and $\bar{\tilde{f}}$:

$$\bar{F} = \langle \rho \rangle \bar{\tilde{f}} / J_x. \tag{65}$$

Thus, as previously noted, Eq. (15) is valid only in Cartesian coordinate systems.

III.2. *Pdf Equation Transformations*

To transform the pdf evolution equation from Cartesian to non-Cartesian coordinates, it is most expedient to work with the mdf and then to use Eq. (65) to relate the transformed mdf to the transformed pdf. In Cartesian coordinates, the equation for $F(\mathbf{V}, \Psi, \mathbf{x}; t)$ corresponding to Eqs. (21)–(23) or to Eqs. (24)–(26) can be written as [14]

$$\frac{\partial F}{\partial t} + V_i \frac{\partial F}{\partial x_i} = \chi, \tag{66}$$

where χ represents, collectively, the mean pressure gradient term, the body force term, the scalar source term, and the modeled terms in the mdf equation. These

terms represent transport of the mdf in velocity and composition space (Eq. (19)). The observation that χ inolves no transport of the mdf in physical space greatly simplifies the task of transforming Eq. (66). In the transformed coordinate system, this term is the same as in a Cartesian system that is locally aligned with $\bar{\mathbf{x}}$. Then for all consistent models (i.e., those that satisfy the modeling principles of dimensional consistency and coordinate system independence [14], such as those introduced in Section II of this paper), χ transforms, simply, by

$$J\bar{\chi} = \chi. \tag{67}$$

All that remains, then, is to transform the model-independent left-hand side of Eq. (66). These terms can be transformed directly to yield an evolution equation for $\bar{F}$, but the algebra is tedious and provides little motivation for the development of the Monte Carlo solution algorithm. It is simpler and more informative to use a Lagrangian approach.

The transformation can be obtained simply by considering the particle equations

$$\dot{x}_i^* = U_i^*, \qquad \dot{U}_i^* = 0, \qquad \dot{\Phi}^* = 0, \tag{68}$$

in a Cartesian coordinate system (i.e., Eqs. (24)–(26) without the terms that contribute to χ in Eq. (66)). This leads to [14] the corresponding mdf equation

$$\frac{\partial F}{\partial t} + V_i \frac{\partial F}{\partial x_i} = 0. \tag{69}$$

For a non-Cartesian system, we apply the transformations of Eqs. (56), (57), and (58) to Eq. (68) to obtain

$$\dot{\bar{x}}_i^* = \frac{\bar{U}_i^*}{\mu h_{(i)}}, \qquad \dot{\bar{U}}_i^* = C_i, \qquad \dot{\bar{\Phi}}^* = 0. \tag{70}$$

The transport equation for $\bar{F}$ follows directly from Eq. (70), using Eq. 4.39 of Ref. [14]:

$$\frac{\partial \bar{F}}{\partial t} + \bar{V}_i \frac{\partial}{\partial \bar{x}_i}\left[\frac{\bar{F}}{\mu(\bar{\mathbf{x}})\, h_{(i)}(\bar{\mathbf{x}})}\right] + \frac{\partial}{\partial \bar{V}_i}\left[\bar{F} C_i(\bar{\mathbf{x}}, \bar{\mathbf{V}})\right] = 0. \tag{71}$$

Substitution of Eq. (65) into Eq. (71) then yields

$$\frac{\partial(\langle\rho\rangle \bar{\tilde{f}})}{\partial t} + J_x \bar{V}_i \frac{\partial}{\partial \bar{x}_i}\left[\frac{\langle\rho\rangle \bar{\tilde{f}}}{\mu h_{(i)} J_x}\right] + \frac{\partial}{\partial \bar{V}_i}\left[\langle\rho\rangle \bar{\tilde{f}} C_i\right] = 0. \tag{72}$$

This is the required transformed pdf equation. We now show that this equation is consistent with conservation of mass in the new coordinate system.

Integration of Eq. (72) over all velocity–composition space gives

$$\frac{\partial\langle\rho\rangle}{\partial t}+J_x\frac{\partial}{\partial\bar{x}_i}\left[\frac{\langle\rho\rangle\,\bar{\tilde{U}}_i}{\mu h_{(i)}J_x}\right]=0, \tag{73}$$

which can be recast in the form (Eqs. (8) and (60))

$$\frac{\partial\langle\rho\rangle}{\partial t}+\frac{1}{h_1h_2h_3}\frac{\partial}{\partial\bar{x}_i}\left[\frac{\langle\rho\mu^{-1}\bar{U}_i\rangle\,h_1h_2h_3}{h_{(i)}}\right]=0. \tag{74}$$

Recalling that $\mu^{-1}\bar{U}_i$ is the physical component of the velocity in the $\bar{x}_i$ direction, it may be seen that Eq. (74) is the mean continuity equation in the curvilinear coordinate system (see Appendix 2 of Ref. [24]), i.e.,

$$\frac{\partial\langle\rho\rangle}{\partial t}+\nabla\cdot\langle\rho\mathbf{U}\rangle=0. \tag{75}$$

This serves as a consistency check on Eq. (72); it demonstrates that the spatial derivatives in that equation are in the proper divergence form.

The time derivative and convective transport in physical space terms of the pdf equation have now been transformed to general orthogonal coordinate systems. The term $J^{-1}\cdot\chi$ (Eq. (67)) is added to the right-hand side of Eq. (71) to complete the transformation of the mdf equation; and, the term $J_U^{-1}\cdot\chi$ (Eqs. (62), (65), and (67)) is added to the right-hand side of Eq. (72) to complete the transformation of the density-weighted pdf equation.

III.3. *Monte Carlo Method*

The next step is to construct a Monte Carlo algorithm for the solution of Eq. (72). To this end, we first recall that the primary motivation for introducing non-Cartesian coordinates is to reduce the dimensionality of the problem in physical space, i.e., such that $\partial(\langle\rho\rangle\bar{\tilde{f}})/\partial\bar{x}_i=0$ for some i. For a statistically D-dimensional flow, it is possible to order the $\bar{x}_i$ such that $\partial(\langle\rho\rangle\bar{\tilde{f}})/\partial\bar{x}_i=0$ for the last $3-D$ i's. With this ordering, we define

$$y_i=\bar{x}_i, \qquad i=1,\ldots,D \qquad (D\leqslant 3), \tag{76}$$

and

$$z_i=\bar{x}_{i+D}, \qquad i=1,\ldots,3-D. \tag{77}$$

Thus for a statistically one-dimensional flow, $(\bar{x}_1,\bar{x}_2,\bar{x}_3)=(y_1,z_1,z_2)$; for a statistically two-dimensional flow, $(\bar{x}_1,\bar{x}_2,\bar{x}_3)=(y_1,y_2,z_1)$; and, for a statistically three-dimensional flow, $(\bar{x}_1,\bar{x}_2,\bar{x}_3)=(y_1,y_2,y_3)$. By definition, $\partial(\langle\rho\rangle\bar{\tilde{f}})/\partial z_i=0$. In general, although $\langle\rho\rangle\bar{\tilde{f}}$ is independent of $\mathbf{z}$, μ, J_x, and $\bar{F}$ can still depend upon $\mathbf{z}$. Hence, for definiteness we take $\mathbf{z}$ to be fixed at some arbitrary value.

We appeal to a Lagrangian approach, and seek a Monte Carlo solution in terms of the particle properties $\mathbf{y}^*(t)$, $\bar{\mathbf{U}}^*(t)$, $\bar{\Phi}^*(t)$ and $w^*(t)$, where $w^*(t)$ is a particle

weight (as yet unspecified). It is not necessary to carry the particle locations in the homogeneous directions ($\mathbf{z}$) in the computations. By analogy with Eqs. (37) and (39), we introduce a delta function discrete representation

$$G(\bar{\mathbf{V}}, \bar{\Psi}, \mathbf{y}; t) \equiv \langle w^*(t)\, \delta(\bar{\mathbf{V}} - \bar{\mathbf{U}}(t))\, \delta(\bar{\Psi} - \bar{\Phi}^*(t))\, \delta(\mathbf{y} - \mathbf{y}^*(t)) \rangle. \tag{78}$$

We then require that G be a consistent representation of $\bar{f}$ in the sense that, for a specified positive density $\lambda(\mathbf{y})$,

$$G(\bar{\mathbf{V}}, \bar{\Psi}, \mathbf{y}; t) \equiv \langle \rho \rangle \bar{f}(\bar{\mathbf{V}}, \bar{\Psi}; \bar{\mathbf{x}}, t)\, \lambda(\mathbf{y}) = \bar{F}(\bar{\mathbf{V}}, \bar{\Psi}, \bar{\mathbf{x}}; t)\, J_x \lambda(\mathbf{y}). \tag{79}$$

We consider the general particle evolution equations

$$\dot{\mathbf{y}} = \hat{\mathbf{U}}(\bar{\mathbf{x}}^*, \bar{\mathbf{U}}^*), \tag{80}$$

$$\dot{\mathbf{U}}^* = \hat{\mathbf{A}}(\bar{\mathbf{x}}^*, \bar{\mathbf{U}}^*), \tag{81}$$

$$\dot{w} = \Omega(\bar{\mathbf{x}}^*, \bar{\mathbf{U}}^*)\, w(t), \tag{82}$$

and deduce the unknowns $\hat{\mathbf{U}}$, $\hat{\mathbf{A}}$, and Ω by requiring that Eq. (79) be satisfied.

The transport equation for G of Eq. (78), with particle properties evolving by Eqs. (80)–(82), is derived from first principles [14]:

$$\frac{\partial G}{\partial t} + \frac{\partial [G \hat{U}_i(\bar{\mathbf{x}}, \bar{\mathbf{V}})]}{\partial y_i} + \frac{\partial [G \hat{A}_i(\bar{\mathbf{x}}, \bar{\mathbf{V}})]}{\partial \bar{V}_i} - \Omega(\bar{\mathbf{x}}, \bar{\mathbf{V}})\, G = 0. \tag{83}$$

Next, we substitute $G = \langle \rho \rangle \bar{f} \lambda$ (Eq. 79) to obtain the corresponding pdf equation:

$$\frac{\partial (\langle \rho \rangle \bar{f})}{\partial t} + \frac{\partial (\langle \rho \rangle \bar{f} \hat{U}_i)}{\partial y_i} + \frac{\langle \rho \rangle \bar{f} \hat{U}_i}{\lambda} \frac{\partial \lambda}{\partial y_i} + \frac{\partial (\langle \rho \rangle \bar{f} \hat{A}_i)}{\partial \bar{V}_i} - \Omega \langle \rho \rangle \bar{f} = 0. \tag{84}$$

Upon comparison of Eqs. (72) and (84), it may be seen that consistency of these two equations demands that the right-hand side of the particle evolution equations (Eqs. (80)–(82)) be

$$\hat{U}_i = \frac{\bar{U}_i^*}{\mu h_{(i)}}, \tag{85}$$

$$\hat{A}_i = C_i, \tag{86}$$

$$\Omega = \frac{\bar{U}_i^*}{\mu h_{(i)}} \left[\frac{1}{\lambda} \frac{\partial \lambda}{\partial y_i} + \frac{1}{J_x} \frac{\partial J_x}{\partial \bar{x}_i} + \frac{1}{\mu h_{(i)}} \frac{\partial (\mu h_{(i)})}{\partial z_i} \right]. \tag{87}$$

The choice of λ is not unique: any positive $\lambda(\mathbf{y})$ may selected, as long as the appropriate weight evolution is used. If there are no deleted coordinates, then $\lambda = J_x^{-1}$ is the obvious choice, since this gives $\Omega = 0$. In general, the best choice for $\lambda(\mathbf{y})$ appears to be $\lambda = J_y^{-1}$, where J_y is the Jacobian J_x with arbitrary fixed values

for the deleted coordinates $\mathbf{z}$. Then $\lambda(\mathbf{y})$ is proportional to the inverse of a volume in $\mathbf{y}$ space, and it transforms as a density, consistent with its definition in Eq. (79).

A physical interpretation of the particle weights may be deduced as follows. The quantity w^*/λ has dimensions of a mass times a volume in $\mathbf{y}$ space divided by a volume in Cartesion ($\mathbf{x}$) space (Eqs. (78) and (79)). Thus w^*/λ is the volume density of mass represented by a particle, independent of the choice of $\lambda(\mathbf{y})$, and $w^*/(\lambda J_y)$ is the mass of fluid represented by a particle. If we choose $\lambda(\mathbf{y}) = J_y^{-1}$, then w^* itself is the particle mass.

We now have a discrete representation that is consistent with the modeled pdf evolution equation in non-Cartesian coordinates. As was done in Section II for Cartesian systems, we next relate the particle properties to the density-weighted pdf $\tilde{f}$. Integrating G (Eq. (78)) over all velocity–composition space yields

$$\langle w^* \delta(\mathbf{y} - \mathbf{y}^*(t)) \rangle = \langle \rho \rangle \lambda(\mathbf{y}). \tag{88}$$

It can also be shown [5, 14] that the left-hand side of Eq. (88) is equal to the conditional expectation of w^*, given that $\mathbf{y}^* = \mathbf{y}$, multiplied by the pdf of particle locations, denoted by $l(\mathbf{y})$:

$$\langle w^* \delta(\mathbf{y} - \mathbf{y}^*(t)) \rangle = \langle w^* \mid \mathbf{y}^* = \mathbf{y} \rangle \, l(\mathbf{y}). \tag{89}$$

It follows from Eqs. (88) and (89) that the pdf of particle positions $l(\mathbf{y})$ is related to the particle weights w^*, to $\lambda(\mathbf{y})$, and to the mean fluid density $\langle \rho \rangle$ by

$$l(\mathbf{y}) = \frac{\langle \rho \rangle \lambda(\mathbf{y})}{\langle w^* \mid \mathbf{y}^* = \mathbf{y} \rangle}. \tag{90}$$

Thus any two of the three quantities $l(\mathbf{y})$, $\lambda(\mathbf{y})$, and $\langle w^* \mid \mathbf{y}^* = \mathbf{y} \rangle$ may (initially) be chosen arbitrarily. Equation (90) is consistent with the interpretation of w^*/λ as the volume density of mass represented by a particle.

By analogy with Eq. (45), the pdf of particle properties at a fixed location $\mathbf{y}^* = \mathbf{y}$ is given by

$$f^*(\bar{\mathbf{V}}, \bar{\Psi}; t \mid \mathbf{y}^* = \mathbf{y}) = \frac{\langle w^*(t) \, \delta(\bar{\mathbf{V}} - \tilde{\mathbf{U}}^*(t)) \, \delta(\bar{\Psi} - \bar{\Phi}^*(t)) \, \delta(\mathbf{y} - \mathbf{y}^*(t)) \rangle}{\langle w^*(t) \, \delta(\mathbf{y} - \mathbf{y}^*(t)) \rangle}. \tag{91}$$

The numerator is $\langle \rho \rangle \tilde{f} \lambda$ (Eqs. (78) and (79)) and the denominator is $\langle \rho \rangle \lambda$ (Eq. (88)), so that

$$f^*(\bar{\mathbf{V}}, \bar{\Psi}; t \mid \mathbf{y}^* = \mathbf{y}) = \tilde{f}(\bar{\mathbf{V}}, \bar{\Psi}; \bar{\mathbf{x}}, t). \tag{92}$$

Thus, as in the Cartesian algorithm, the distribution of particles in velocity–composition space at a fixed position is equal to the density-weighted joint pdf.

With Eq. (92), we can derive the evolution equation for the particle number density $l(\mathbf{y}) = \langle \delta(\mathbf{y} - \mathbf{y}^*(t)) \rangle$:

$$\frac{\partial l}{\partial t} = -\frac{\partial}{\partial y_i}\left[l(\mathbf{y})\,\langle \dot{y}_i^* \mid \mathbf{y}^* = \mathbf{y}\rangle\right] = -\frac{\partial}{\partial y_i}\left[l(\mathbf{y})\left\langle \frac{\bar{U}_i^*}{\mu h_{(\iota)}} \mid \mathbf{y}^* = \mathbf{y}\right\rangle\right]$$
$$= -\frac{\partial}{\partial y_i}\left[l(\mathbf{y})\frac{\tilde{\bar{U}}_i}{\mu h_{(\iota)}}\right]. \tag{93}$$

Here we have made use of Eqs. (80) and (85) and the result of Eq. (92), which says that averages of particle properties at a fixed spatial location are equal to density-weighted means. If there are no deleted coordinates, Eq. (93) reduces to the mean continuity equation (Eq. (73)), but with lJ_x in place of $\langle \rho \rangle$. From this it follows that if if l is initially set proportional to $\langle \rho \rangle / J_x$, then l remains proportional to the local value of $\langle \rho \rangle / J_x$ for all time. In general, however, we are free to choose the initial particle number density $l(\mathbf{y})$ and either the initial particle weights w^* or the density $\lambda(\mathbf{y})$ in any convenient manner. Independent of this choice, $l(\mathbf{y})$ evolves in time according to Eq. (93). When there are deleted coordinates, there may be no

As is the case for Cartesian coordinates, satisfying the mean continuity equation guarantees that $\bar{F}$ remains a valid mdf for all time, given that it is valid initially; the discrete representation of Eq. (78) remains a valid representation of $\bar{F}$ for all time for any choice of $\lambda(\mathbf{y})$, provided that the particle weights evolve according to Eqs. (82) and (87); and, the particle number density in physical space evolves by Eq. (93) and satisfies Eq. (90) for all time under these conditions.

From Eqs. (78) and (79) and the discussion following Eq. (87), it follows that mass-weighted ensemble averages over particles at a fixed location in physical space are estimates of Favre averages. Consider a subregion of physical space of volume V_k centered at $\mathbf{y}_k$ and containing N_k particles. If this volume is sufficiently small so that variations in mean quantities are negligible inside of it, then

$$\tilde{Q}(\mathbf{y}_k) \approx \tilde{Q}_{N_k}(\mathbf{y}_k) = \frac{1}{N_k}\sum \frac{w^{(n)}}{\lambda(\mathbf{y}^{(n)})\,J_y(\mathbf{y}^{(n)})}\,Q(\bar{\mathbf{V}}^{(n)}, \Psi^{(n)}) \Big/ \frac{1}{N_k}\sum \frac{w^{(n)}}{\lambda(\mathbf{y}^{(n)})\,J_y(\mathbf{y}^{(n)})}, \tag{94}$$

where the summation is over the N_k particles in cell k. The statistical error in this approximation is of order $N_k^{-1/2}$, by the same reasoning that let to Eqs. (49) and (50).

In the Monte Carlo solution algorithm, we solve the particle equations (Eqs. (80)–(82) with Eqs. (85)–(87)), adding the transformed terms $\mu a_{ij} A_j^*$ and B^* (Eqs. (25), (26), (56), and (58)) to the $\dot{\bar{U}}_i^*$ and $\dot{\bar{\Phi}}^*$ equations, respectively. We solve at arbitrary fixed values of the deleted coordinates $\mathbf{z}$. Particle positions in directions of homogeneity of $\langle \rho \rangle \tilde{f}$ need not be carried in the computations. The density $\lambda(\mathbf{y})$ is chosen to be J_y^{-1}. The initial distribution of particle positions is taken to be proportional to the mean fluid density; Eq. (90) then shows that the initial particle weights w^* are proportional to J_y^{-1}. Particle initial velocities and compositions are

set to correspond to the initial density-weighted joint pdf (Eq. (92)). The D-dimensional physical space is divided into K cells, the kth being centered at $\mathbf{y}_k$ with a

over particles within each cell (Eq. (94)) can be used to extract profiles of mean quantities as a function of $\mathbf{y}$ from the numerical solution; in practice, however, the statistical error is too large. A more satisfactory method of extracting means from the solution is a curve-fitting technique, cross-validated least-squares cubic splines with smoothing [14, 25]. For Favre averaging, each particle is assigned a weight $w^*/(\lambda J_y) = w^*$ in forming the splines. Using this technique, we expect that the statistical error for any local function of the velocity and scalar fields scales as $N^{-1/2}$. Numerical tests confirming this assertion are presented in Section V.

To keep the spline-fitting well conditioned, it is desirable to prevent particle weights from becoming excessively large or small in the course of the calculations. Ideally, we would like to have equal particle weights within each cell. It may seen from Eq. (94) that particle weights can be modified in many ways that leave weighted averages unaltered. For example, the weights of all particles can be multiplied by any constant (or by any function of the deleted coordinates $\mathbf{z}$); particles can be "cloned," i.e., a particle of weight w can be split into two particles of weight $w/2$ with the same properties at the same physical location; and, particles of weight w, less than some preferred weight $\hat{w}$, can be "annihilated," or removed, with probability $1 - w/\hat{w}$ and "promoted" from weight w to weight $\hat{w}$ with probability $w/\hat{w}$, with only a small statistical error. These ideas are used to keep particle weights within each cell more or less uniform.

III.4. *Summary*

Rules for transforming pdf equations from Cartesian to general orthogonal coordinates have been presented, and a discrete representation has been devised that forms the basis for the Monte Carlo solution algorithm in the transformed coordinate system. The essential ingredients of the development are that, first, a Lagrangian viewpoint is adopted and, second, a time-dependent weight is included in the discrete representation of the pdf. Particle weights evolve to account for the change in fluid mass or volume represented by a particle as it moves in the non-Cartesian coordinates. This evolution renders the discrete representation consistent with the modeled pdf equation. The algorithm described above for general orthogonal coordinates reduces in a straightforward way to the algorithm described in Section II for Cartesian systems.

IV. Application to Self-Similar Free Shear Flows

We now consider three specific flows. These serve to make the general treatment given so far more concrete, as well as to provide a means of solving the modeled pdf evolution equation for three important turbulent free shear flows. Coordinate system transformations for these flows appear in the Appendix. All of the flows con-

sidered are of uniform density, so that it is not necessary to carry the scalar evolution equation: the solved for pdf is the joint pdf of the velocities $\tilde{f}(\bar{\mathbf{V}}; \bar{\mathbf{x}}, t)$. The numerical algorithm is outlined briefly, and some remarks are made concerning the earlier pseudo-Cartesian algorithms used in Refs. [12, 13].

These self-similar flows spread linearly with x [26], so that in each case, statistics of suitably scaled velocity components are independent of radial distance from the virtual origin of the flow. (Strictly speaking, self-similarity of the governing equations is only possible in the limit as the Reynolds number approaches infinity, so that viscosity has a negligible direct effect on the mean flow [27]. However, it is customary in the turbulence literature to refer to flows where suitably normalized profiles of mean quantities become independent of the streamwise coordinate as "self-similar" or "self-preserving," and we shall do the same here.)

IV.1. *Self-Similar Plane Mixing Layer*

The two-dimensional mixing region between two uniform parallel irrotational streams is sketched in Fig. 1. A convenient coordinate system in which to study this flow is the cylindrical system shown there. It can be demonstrated analytically that for any value of the velocity ratio $V_R \equiv U_L/U_H$, the equations of the mean motion for this flow admit a self-preserving solution where the statistics of the velocities are independent of r; this self-preserving solution is observed to exist in experiments as well [26].

We adopt the coordinates $\bar{\mathbf{x}} = \{r, \theta, z\}$, $\bar{\mathbf{U}} = \{U_r, U_\theta, U_z\}$, where U_r, U_θ, and U_z are the physical components of the velocity in the r, θ, and z directions, respectively. Thus the stretching factor is unity ($\mu = 1$, Eq. (55)). The relevant joint pdf is $\tilde{f}(V_r, V_\theta, V_z; r, \theta, z, t)$. This flow is statistically homogeneous in the z direction so that $\tilde{f}$ is independent of z; self-similarity implies that $\tilde{f}$ is independent of r as well. In the notation of Section III, the particle evolution equations are

$$\dot{y}_1^* = \dot{\theta}^* = U_\theta^*/r^*, \tag{95a}$$

$$\dot{z}_1^* = \dot{r}^* = U_r^*, \tag{95b}$$

$$\dot{z}_2^* = \dot{z}^* = U_z^*, \tag{95c}$$

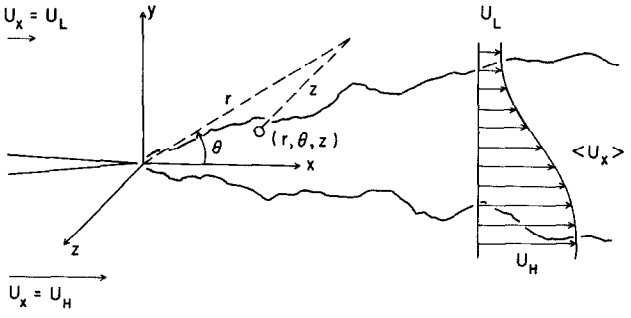

FIG. 1. The turbulent plane mixing layer.

$$\dot{U}_r^* = U_\theta^{*2}/r^* + \bar{A}_r^*, \tag{95d}$$

$$\dot{U}_\theta^* = -U_r^* U_\theta^*/r^* + \bar{A}_\theta^*, \tag{95e}$$

$$\dot{U}_z^* = \bar{A}_z^*, \tag{95f}$$

where the $\bar{\mathbf{A}}^*$ terms are the transformed mean pressure gradient and modeled terms (Eqs. (22) and (25)). Since $J_x = 1/r$ is independent of θ, we simply take $\lambda = 1$; Eqs. (82) and (87) then show that particle weights must evolve by

$$\dot{w}^* = -U_r^* w^*/r^*. \tag{96}$$

IV.2. *Self-Similar Plane Jet*

Figure 2 depicts a turbulent jet issuing from a two-dimensional slot into stagnant surroundings. Analysis and experiment reveal that this flow becomes self-preserving sufficiently downstream of the slot [26]. We again adopt the cylindrical coordinate system used for the self-similar plane mixing layer. Here, however, it is the statistics of $U_r' = r^{1/2}U_r$, $U_\theta' = r^{1/2}U_\theta$, and $U_z' = r^{1/2}U_z$ that are independent of r in the self-similar regime, so that $\bar{\mathbf{U}} = \mathbf{U}' = \{U_r', U_\theta', U_z'\}$ is the most convenient choice of velocity components. Thus $\mu = r^{1/2}$ here. The joint pdf $\tilde{f}(V_r', V_\theta', V_z'; r, \theta, z, t)$ is then independent of z through statistical homogeneity and independent of r via self-similarity. Taking $\lambda = 1$ again, the transformed particle equations read

$$\dot{y}_1^* = \dot{\theta}^* = U_\theta'^*/r^{*3/2}, \tag{97a}$$

$$\dot{z}_1^* = \dot{r}^* = U_r'^*/r^{*1/2}, \tag{97b}$$

$$\dot{z}_2^* = \dot{z}^* = U_z'^*/r^{*1/2}, \tag{97c}$$

$$\dot{U}_r'^* = (U_\theta'^{*2} + \tfrac{1}{2}U_r'^{*2})/r^{*3/2} + \bar{A}_r^*, \tag{97d}$$

$$\dot{U}_\theta'^* = -\tfrac{1}{2}U_r'^* U_\theta'^*/r^{*3/2} + \bar{A}_\theta^*, \tag{97e}$$

$$\dot{U}_z'^* = \tfrac{1}{2}U_r'^* U_z'^*/r^{*3/2} + \bar{A}_z^*, \tag{97f}$$

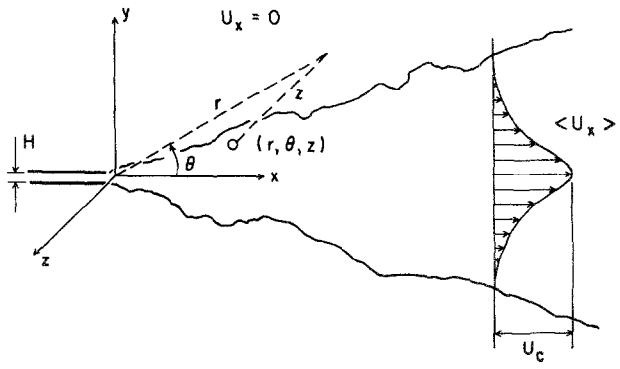

FIG. 2. The turbulent plane jet.

and

$$\dot{w}^* = -\tfrac{1}{2} U_r'^* w^* / r^{*3/2}. \tag{98}$$

IV.3. *Self-Similar Axisymmetric Jet*

An axisymmetric turbulent jet issuing from a nozzle of diameter D into stagnant surroundings is shown in Fig. 3. We select the spherical coordinate system $\tilde{\mathbf{x}} = \{r, \phi, \theta\}$ for the treatment of this flow (Fig. 3). Then analysis and experiment show that the flow achieves a self-preserving state where the statistics of $\bar{\mathbf{U}} = \mathbf{U}' = \{rU_r, rU_\phi, rU_\theta\}$ become independent of r [26], so that $\mu = r$ here. The joint pdf $\bar{f}(V_r', V_\phi', V_\theta'; r, \phi, \theta, t)$ is then independent of θ (axisymmetry) and independent of r (self-similarity). We again write the transformed particle position and velocity equations in the notation of Section III,

$$\dot{y}_1^* = \dot{\phi}^* = U_\phi'^*/r^{*2}, \tag{99a}$$

$$\dot{z}_1^* = \dot{r}^* = U_r'^*/r^*, \tag{99b}$$

$$\dot{z}_2^* = \dot{\theta}^* = U_\theta'^*/(r^{*2} \sin \phi^*), \tag{99c}$$

$$\dot{U}_r'^* = (U_r'^{*2} + U_\phi'^{*2} + U_\theta'^*)/r^{*2} + \bar{A}_r^*, \tag{99d}$$

$$\dot{U}_\phi'^* = U_\theta'^{*2}/(r^{*2} \tan \phi^*) + \bar{A}_\phi^*, \tag{99e}$$

$$\dot{U}_\theta'^* = -U_\phi'^* U_\theta'^*/(r^{*2} \tan \phi^*) + \bar{A}_\theta^*, \tag{99f}$$

and taking $\lambda = \sin \phi$ (i.e., proportional to $J_x^{-1} = r^2 \sin \phi$ with r fixed at an arbitrary value), particle weights evolve by

$$\dot{w}^* = -U_r'^* w^*/r^{*2}. \tag{100}$$

IV.4. *Solution Algorithm*

Each of the three self-similar flows has been reduced to a statistically one-dimensional problem in physical space by an appropriate choice of coordinate system.

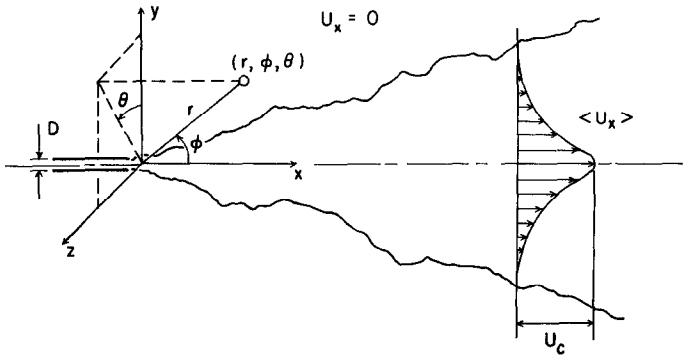

FIG. 3. The turbulent axisymmetric jet.

Particles exist in the four-dimensional state space $\{y, \bar{V}_1, \bar{V}_2, \bar{V}_3\}$, where y denotes the single retained physical coordinate. Since the radial particle positions are not carried in the calculation, we may solve at any convenient radius; we choose $r = 1$. The y space is divided into K equally spaced cells of width Δy, the kth being centered at y_k. Particles are initially distributed uniformly in y and the initial weights w^* of particles within each cell are proportional to $\lambda(y_k)$ (Eq. (90)). For the flows

$\lambda(y_k) = \sin(y_k)$. Initial particle velocities are (almost) arbitrary since we are interested only in the statistically stationary self-preserving solution. Profiles of mean velocities, the components of the covariance matrix (Reynolds stresses) as functions of y, and other statistics of interest are extracted using the splines mentioned in Section III. We march in time using a discretized form of the particle evolution equations (a first-order scheme for the Langevin model was described in Section II) until self-preservation is achieved, that is, until normalized profiles of mean quantities become independent of time.

IV.5. *Pseudo-Cartesian Algorithms*

It was mentioned in Section I that the flows treated in Refs. [12, 13] were, respectively, in cylindrical and spherical coordinates. Pope and Correa [12] solved for an axisymmetric jet diffusion flame while Pope and Cheng [13] studied a spherically symmetric premixed flame. Yet in both cases, an essentially Cartesian solution algorithm was used. Each particle was initially assigned a weight proportional to the mass of fluid that it represents, and the weights then remain fixed.

The essential difference between these two flows and the flows discussed earlier in this section is the orientation of the directions of homogeneity. For the jet diffusion flame, a cylindrical coordinate system is adopted with the flow axis in the z direction and statistical homogeneity in the θ direction (see Fig. 1). We then have $y_1 = r$, $y_2 = z$, and $z_1 = \theta$. Physical components of the velocities are used, so that $\mu = 1$. With $\lambda = J_y^{-1} = r$, Eqs. (82) and (87) show that $\dot{w}^* = 0$. For the spherical diffusion flame, there is statistical homogeneity in ϕ and θ (see Fig. 3). We again use the physical velocity components: $y_1 = r$, $z_1 = \phi$, $z_2 = \theta$, and $\mu = 1$. Here $\lambda = J_y^{-1} = r^2$, so Eqs. (82) and (87) yield $\dot{w}^* = -U_\phi^* w^*/(r^* \tan \phi^*)$. However, the marginal pdf of the ϕ velocity, $\tilde{f}(V_\phi; r, t)$, is symmetric about $V_\phi = 0$; weighted averages (Eq. (94)) are then independent of the evolution of w^* due to U_ϕ^*, so it is legitimate to simply set $\dot{w}^* = 0$. These pseudo-Cartesian algorithms are discussed further in Ref. [14].

V. Numerical Tests

The results of two types of numerical tests are reported. First, the spreading rate of the self-similar plane mixing layer is calculated using three numerical algorithms. The first is the new self-similar algorithm developed in Section IV, and the other two are the Cartesian algorithms developed in Ref. [14]. A comparison of these

three methods of calculation serves both to validate the new approach introduced in this paper and to expose the limitations of the other techniques. Second, the statistical error as a function of the number of particles N is calculated and compared to standard error estimates, demonstrating convergence of the Monte Carlo algorithm.

These computations are intended as numerical tests only, not as a modeling study of the plane mixing layer: no comparisons with experimental data are presented. A modeling study of self-similar turbulent free shear flows using the ideas developed in this paper may be found in Ref. [28].

V.1. *Comparison of Algorithms*

We now let $\mathbf{x} = \{x, y, z\}$ and $\mathbf{U} = \{U_x, U_y, U_z\}$. A characteristic velocity difference ΔU for the plane mixing layer is

$$\Delta U \equiv U_H - U_L, \tag{101}$$

(see Fig. 1) and we define a characteristic width δ in terms of the points on the mean velocity profile where the mean velocity is $U_L + 0.2(U_H - U_L)$ and $U_L + 0.8(U_H - U_L)$. Denoting these points by $y_{0.2}$ and $y_{0.8}$, respectively, the width δ is defined to be

$$\delta \equiv y_{0.2} - y_{0.8}. \tag{102}$$

A similarity coordinate η for the mxing layer can be defined as

$$\eta = \frac{y - y_{0.5}}{\delta} = \frac{y - y_{0.5}}{y_{0.2} - y_{0\,8}}, \tag{103}$$

where $y_{0.5}$ is defined analogously with $y_{0.2}$ and $y_{0.8}$. Self-similarity implies that profiles of any one-point statistic of the Eulerian velocity field (normalized by ΔU) become a function of η only, independent of x. It can be shown that for the self-similar plane mixing layer, the spreading rate S is a constant, where S is given by [26]

$$S = d\delta/dx. \tag{104}$$

An important parameter is the velocity ratio V_R defined by

$$V_R \equiv U_L/U_H. \tag{105}$$

Since $0 \leqslant U_L \leqslant U_H$, V_R takes on values between zero and one, inclusive.

The three solution techniques are designated as method 1, method 2, and method 3. Method 1 is the self-similar algorithm developed in Section IV; it is valid for all V_R. Method 2 is a boundary-layer algorithm that was presented in Ref. [14]; it is limited to higher values of V_R. The final technique, method 3, is the time-dependent algorithm developed in Ref. [14] and described at the end of Section II; it is restricted to the limiting case $V_R \to 1$.

In method 1, we solve in a cylindrical coordinate system and march the solution in time until self-similarity is achieved. Since the turbulent plane mixing layer is self-similar for any value of the velocity ratio V_R, this method is equally valid for all velocity ratios.

Method 2 treats the mixing layer as a statistically stationary two-dimensional flow using the boundary-layer algorithm developed in Ref. [14]. This is a modification of the basic Cartesian algorithm described in Section II; each particle represents a fixed axial momentum of fluid rather than a fixed mass. The streamwise step $\Delta x = \Delta x^{(n)}$ is the same for all particles $n = 1,..., N$, and the particle time steps $h^{(n)}$ are given by $\Delta x = U_x^{(n)} h^{(n)}$. Beginning from (almost) arbitrary initial conditions, the solution is marched downstream until self-similarity is attained. Clearly, this method is applicable only to cases where the flow is predominately in the x direction: there must be a negligible probability of $U_x^{(n)}$ being less than or equal to zero so that the time step $h^{(n)}$ for each particle remains positive. We expect, then, that as $U_L/\Delta U$ approaches zero ($V_R \to 0$), this algorithm breaks down. There are additional approximations in method 2, beyond the scope of the current discussion, that are analogous to the usual boundary-layer assumptions for thin free shear flows [26]. These approximations become negligible in the limit $V_R \to 1$. Thus, we expect this boundary-layer algorithm to be valid for high velocity ratios, and to become increasingly inaccurate as the velocity ratio decreases to zero.

Method 3 is the one-dimensional version of the time-dependent Cartesian scheme described in Section II. Only y variations in statistics are accounted for, so we are essentially solving for the temporally growing plane turbulent region of infinite extent in the x and z directions separating the two uniform free streams. This is not physically the same problem as the spatially developing plane mixing layer of Fig. 1. However, in the limit $\Delta U/U_H \to 0$ ($V_R \to 1$), an analogy can be drawn between the spatially developing plane mixing layer and this temporally growing layer, where the equivalent "time" for the spatially developing flow is $t = x/U_H$. Thus, it is legitimate to interpret this time-dependent solution as representing a plane mixing layer in the limit $V_R = 1$. The solution is again marched in time until the self-similar solution is reached.

For all of these comparison runs, the first-order accurate time discretization of the Langevin model is used (Eqs. (33) and (34) for methods 2 and 3, Eqs. (95a), (95d), (95e), (95f), and (96) for method 1). The turbulent time scale τ of Eq. (29) is taken to be uniform across the flow and is related to the mean flow scales simply by

$$\tau = \tau^* \frac{\delta}{\Delta U}, \tag{106}$$

where we take $\tau^* = 10$. Since mean quantities change on a time scale that is of order τ, the numerical time step is fixed by the condition that the particle time steps be a small fraction of τ. It was verified that the discretization error due to the nonzero time step was negligible compared to the statistical error due to finite N for the runs reported here. Approximately 50,000 particles were used for each run. In the

numerical calculations, the velocity ratio is varied by keeping ΔU fixed and changing U_H and U_L to get the desired velocity ratio (methods 1 and 2 only). Thus, we can only approach (but never attain) a velocity ratio of unity for methods 1 and 2. Also, we can only approach a velocity ratio of zero for method 2, since U_L cannot be equal to zero in this algorithm. It is expected that method 1 should give correct results for all velocity ratios $0 \leqslant V_R \leqslant 1$; method 2 should be valid at high velocity ratios, with departures from method 1 growing as the velocity ratio as the velocity ratio approaches unity.

For method 2, velocity ratios of 0.90, 0.80, 0.65, 0.50, 0.33, 0.25, 0.20, 0.14, 0.10, and 0.05 were studied; for method 1, these velocity ratios as well as $V_R = 0$ ($U_L = 0$) were included. To compare the spreading rate for the time dependent calculation (method 3) with those of the other two algorithms on an equal footing, it is necessary to use the equivalent "time" mentioned earlier. A normalized spreading rate for the time dependent calculation (method 3) is defined by

$$S_T \equiv \frac{1}{\Delta U} \frac{d\delta}{dt}, \tag{107}$$

and for the spatial calculations (methods 1 and 2), the comparable measure of the spreading is

$$S_X \equiv \frac{U_H}{\Delta U} \frac{d\delta}{dx}. \tag{108}$$

Calculated spreading rates S_X for methods 1 and 2, normalized by S_T of method 3, are plotted as a function of velocity ratio in Fig. 4. As expected, methods 1 and 2 agree for high values of the velocity ratio and diverge at lower velocity ratios as method 2 becomes less and less accurate. For $V_R \geqslant 0.3$, the spreading rates calculated by these two methods are within 10% of each other. At $V_R = 0.2$, the difference is significant, with method 2 giving a spreading rate about 25% lower than method 1. For velocity ratios of 0.25 and lower, the spreading rate calculated by method 2 actually decreases as V_R approaches zero. Both methods 1 and 2 appear to converge to the calculated spreading rate of method 3 as $V_R \to 1$.

Similar results are obtained using models other than the Langevin equation, but the precise velocity ratio at which the boundary-layer algorithm breaks down is different in each case. In the axisymmetric jet diffusion flame of Ref. [12], the particle interaction models described in Ref. [14] were used, together with models that take explicit account of intermittency [7] (that is, the observation that at a fixed point in laboratory coordinates, the flow alternates between turbulent and nonturbulent as the interface separating the turbulent region from the outer irrotational flow moves through that point). Figure 5 shows calculated speading rates vs velocity ratio for the plane mixing layer using these models. It may be seen that the spreading rates calculated by methods 1 and 2 now agree to within 15% for velocity

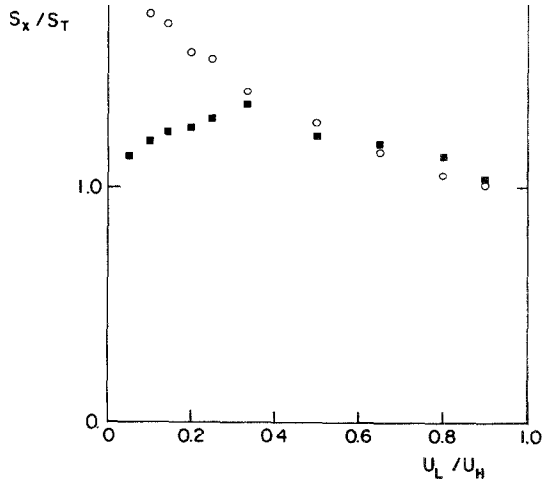

FIG. 4. Calculated spreading rate S_X normalized by S_T of method 3 vs velocity ratio for the turbulent plane mixing layer using the Langevin model. ○, S_X/S_T by method 1; ■, S_X/S_T by method 2.

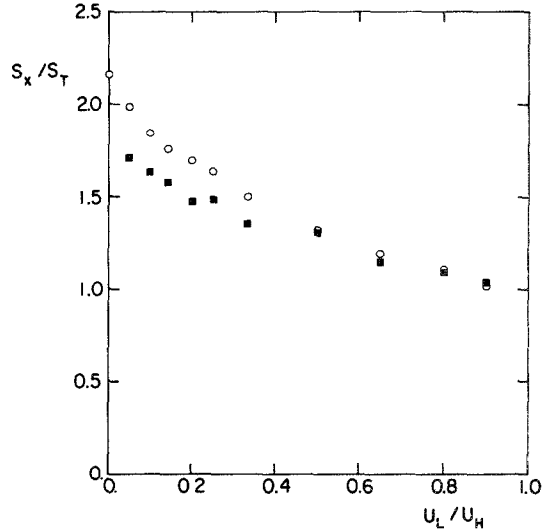

FIG. 5. Calculated spreading rate S_X normalized by S_T of method 3 vs velocity ratio for the turbulent plane mixing layer using particle interaction models with intermittency. ○, S_X/S_T by method 1; ■, S_X/S_T by method 2.

ratios as low as $V_R = 0.05$, and the spreading rate calculated by method 2 continuous to increase with decreasing velocity ratio as $V_R \to 0$. In the jet diffusion flame of Ref. [12], the intitial velocity ratio is $V_R \approx 0.05$ and rapidly increases as the flow evolves. Hence, it is likely that for this flow, the error resulting from the use of the boundary-layer algorithm is within acceptable bounds.

V.2. *Statistical Error*

The statistical error in a Monte Carlo calculation is the error due to the number of particles N being finite. We consider just one quantity from the method 3 Monte Carlo calculations of the plane mixing layer, namely $q \equiv \langle uv \rangle / \Delta U^2$ at $\eta = 0$. Here u and v are the fluctuating components of the streamwise and cross-stream velocities, respectively: $u \equiv U_x - \langle U_x \rangle$ and $v \equiv U_y - \langle U_y \rangle$. In turbulence, $\langle uv \rangle$ is the Reynolds shear stress, an important quantity in free shear flows. The profile of $\langle uv \rangle$ goes to zero at both edges of the mixing layer and has a peak near $\eta = 0$; this quantity is thus a sensitive indicator of the statistical error in the computations. A calculated time series of $\langle uv \rangle / \Delta U^2$ at $\eta = 0$ appears in Fig. 6, where only every tenth time step is shown, for clarity. As expected, there is a transient period as the computations approach self-similarity followed by a stationary regime of random statistical fluctuations about a constant mean.

To quantify the statistical error, we need to study $\langle uv \rangle$ on different time steps on different runs. Hence, we define $q_i^{(r)}(N)$ to be the value of $\langle uv \rangle / \Delta U^2$ from the Monte Carlo calculation (with N particles) at $\eta = 0$, on the ith step for the rth run.

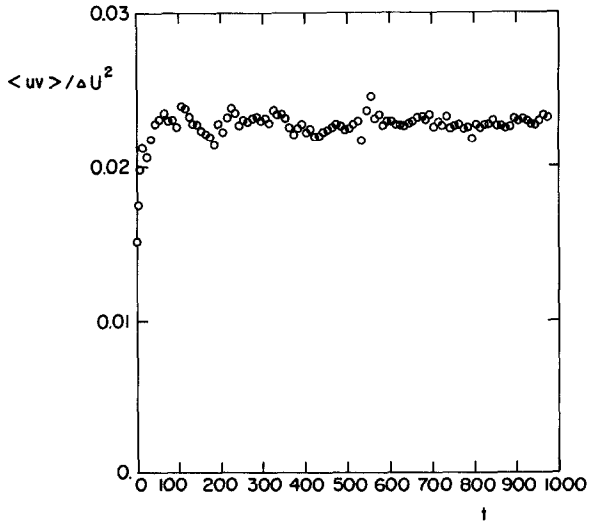

FIG. 6. Calculated time series of the normalized shear stress at $\eta = 0$ for the plane mixing layer, method 3, $N = 50{,}000$.

It is necessary to distinguish between two types of error (see Ref. [15]): the bias b_N is the difference between the mean of $q_i^{(r)}(N)$ and $\langle q \rangle$,

$$b_N \equiv \langle q_i^{(r)}(N) \rangle - \langle q \rangle; \tag{109}$$

the sampling error ε_N is the standard deviation of $q_i^{(r)}(N)$,

$$\varepsilon_N^2 \equiv \mathrm{var}\{q_i^{(r)}(N)\}. \tag{110}$$

The quantity ε_N is a measure of the uncertainty in approximating $\langle q_i^{(r)}(N) \rangle$ by its value on a single time step of a single run, $q_i^{(r)}(N)$.

Both the mean and the variance of $q_i^{(r)}(N)$ can only be estimated from the numerical solution. Averaging over T time steps (starting from step i_1) in the statistically stationary self-similar regime is equivalent to ensemble averaging over several (less than T) independent realizations. The time average for a single run is denoted by $\langle q^{(r)}(N) \rangle_T$,

$$\langle q^{(r)}(N) \rangle_T = \frac{1}{T} \sum_{i=i_1}^{i_1+T} q_i^{(r)}(N). \tag{111}$$

The average of $\langle q^{(r)}(N) \rangle_T$ over R runs, $\langle q(N) \rangle_{T,R}$, is an estimate of $\langle q_i^{(r)}(N) \rangle$:

$$\langle q_i^{(r)}(N) \rangle \approx \langle q(N) \rangle_{T,R} = \frac{1}{R} \sum_{r=1}^{R} \langle q^{(r)}(N) \rangle_T. \tag{112}$$

We use $\langle q(N) \rangle_{T,R}$ as an approximation of $\langle q_i^{(r)}(N) \rangle$ to estimate the bias (Eq. (109)). To ensure the adequacy of this approximation, we need an estimate of the uncertainty in $\langle q(N) \rangle_{T,R}$. For this estimate, we consider the time average over each run to be an independent sample. It then follows that the quantity $\varepsilon_{T,R}$, defined by

$$\varepsilon_{T,R}^2 = \frac{1}{R(R-1)} \sum_{r=1}^{R} (\langle q^{(r)}(N) \rangle_T - \langle q(N) \rangle_{T,R})^2, \tag{113}$$

is the uncertainty in approximating $\langle q_i^{(r)}(N) \rangle$ as $\langle q(N) \rangle_{T,R}$.

In Fig. 7, we plot $\langle q(N) \rangle_{T,R}$ vs $N^{-1/2}$ for different values of N, 12,500, 25,000, 50,000, and 100,000, along with error bars corresponding to $\pm \varepsilon_{T,R}$ (Eq. (113)). In all cases, $T = 300$ and R is chosen so that $\varepsilon_{T,R}$ is about the same for each N, that is, so that the quantity $N \cdot R$ is fixed: the number of runs for each of the above values of N is $R = 48$, 24, 12, and 6. The points labeled *CV-CV* were computed using cross-validated least-squares cubic splines with smoothing for mean quantities (see Refs. [14, 25]). Bias is evident, that is, $\langle q(N) \rangle_{T,R}$ is not independent of N. Two earlier Monte Carlo studies of turbulent flows reported no bias in one case [17] and only a very small bias for small N in the other [29]. In both of these previous calculations, only the pdf of the compositions was treated by a Monte Carlo

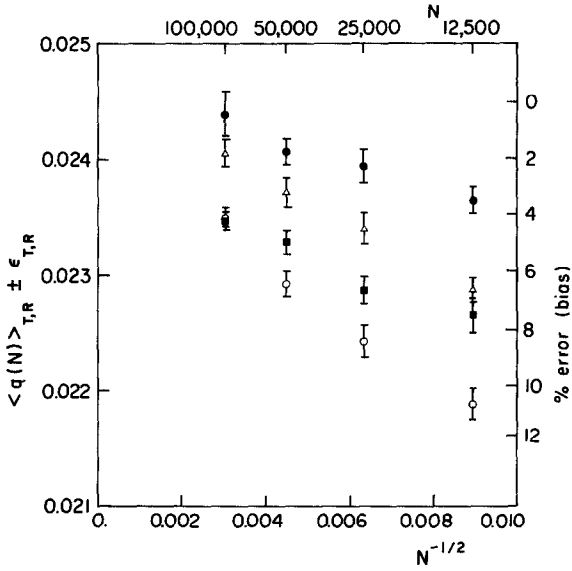

FIG. 7. Expectations of the average of $\langle uv \rangle / \Delta U^2$ at $\eta = 0$ over T time steps and R runs vs $N^{-1/2}$. Error bars show plus and minus the uncertainty $\varepsilon_{T,R}$. Four sets of calculations use different techniques for extracting means from the numerical solution: ○ *CV-CV*; ■ *CV-LS*; △ *LS-CV*; ● *LS-LS*. Percent error is relative to 0.0245.

method. Ensemble averaging was used to extract mean quantties in Ref. [17] while in Ref. [29], cross-validated splines were used.

There are two possible sources of bias in the present calculations. First, the cross-validated splines smooth the curvature of the mean profiles and hence tend to undershoot peaks [25]; the $\langle uv \rangle$ profile has a peak near $\eta = 0$ in this flow. Second, the splined mean quantities k and $\tilde{\mathbf{U}}$ (see Eqs. (27)–(29)) are fed back into the particle equations for the Langevin model used here.

To study this further, three additional sets of calculations were performed; these are labeled *CV-LS*, *LS-CV*, and *LS-LS* in Fig. 7. The first two letters in the label refer to the type of spline used internally in the calculations (that is, for k and $\tilde{\mathbf{U}}$ in Eq. (27)) and the last two letters refer to the type of spline used to extract the output $\langle uv \rangle$: *CV* denotes cross-validated splines with smoothing and *LS* stands for simple least-squares splines without cross-validation. It may be seen from Fig. 7 that both sources of bias are smaller with the least squares splines than with the cross-validated splines. Most of the bias appears to be due to the feedback of splined mean quantities into the calculations.

It is not obvious from Fig. 7 that all four sets of calculations converge to the same value of $\langle uv \rangle / \Delta U^2$ as $N \to \infty$; however, there is no reason to expect that this is not the case. The converged value appears to be 0.0245 ± 0.0003. If we adopt the value $\langle q \rangle = 0.0245$, then Fig. 7 shows that the bias with $N = 12{,}500$ for *CV-CV* is

about 11% while for *LS-LS*, it is about 3%. The small remaining bias using *LS-LS* is presumably due to the feedback of mean quantities into the particle equations.

We now examine the sampling error. The uncertainty in approximating $\langle q_i^{(r)}(N)\rangle$ by a single time step of a single run, i.e., ε_N of Eq. (110), is calculated by

$$\varepsilon_N^2 = \frac{1}{TR}\sum_{r=1}^{R}\left\{\sum_{t=i_1}^{i_1+T}\left[q_i^{(r)}(N) - \langle q(N)\rangle_{T,R}\right]^2\right\}. \tag{114}$$

It is expected that ε_N will increase linearly with $N^{-1/2}$. Figure 8 shows the uncertainty ε_N of Eq. (114) for each of the four sets of calculations. As expected, ε_N increases approximately linearly with $N^{-1/2}$. This figure illustrates that the sampling error is smaller for the cross-validated splines than for the least-squares splines, consistent with the findings of Ref. [25].

In spite of their larger bias, the cross-validated splines are generally preferred because the sampling error may be smaller (Fig. 8) and is independent of the number of basis functions used, by contrast to the least squares method [25]. (Twenty basis functions were used in the present calculations.) This becomes especially important when derivatives of mean quantities are needed [25]. The quantity under consideration, $\langle uv\rangle$, provides a particularly demanding test for the cross-validated splines because of the peak in the vicinity of $\eta = 0$. Figures 7 and 8 together provide evidence for convergence of the numerical solution, since both the bias and the uncertainty appear to go to zero as N approaches infinity.

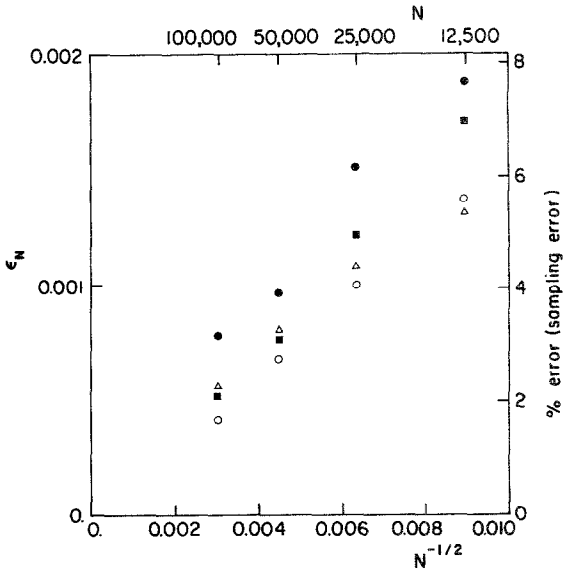

FIG. 8. Uncertainty in estimating $\langle uv\rangle/\Delta U^2$ at $\eta = 0$ by its value at a single time step of one run vs $N^{-1/2}$. Four sets of calculations use different techniques for extracting means from the numerical solution: ○ *CV-CV*; ■ *CV-LS*; △ *LS-CV*; ● *LS-LS*. Percent error is relative to 0.0245.

VI. Conclusions

The pdf method and the Monte Carlo solution algorithm of Ref. [14] have been extended to non-Cartesian coordinate systems and applied to three self-similar turbulent free shear flows of practical interest. The results of numerical tests have been presented, comparing the new method with two earlier Cartesian algorithms for the self-similar plane mixing layer, and demonstrating convergence as the number of particles increases. As in the earlier work, the basis for the modeling and solution of the pdf evolution equation is a Lagrangian viewpoint, in which the bahavior of fluid particles is modeled and the trajectories of fluid particles in the velocity–composition–position state space are calculated. The key to the treatment of non-Cartesian coordinates is the inclusion of a time-dependent particle weight in the discrete representation of the pdf. This weight (divided by λJ_y) is the mass of fluid represented by a particle; it evolves with time because, as the particle moves in the non-Cartesian coordinate system, the physical volume represented by the particle changes.

Non-Cartesian coordinate systems are usually invoked when the boundary conditions or some other physical features of a problem are stated most naturally in such a system. As implied in the selection of the sample problems, curvilinear coordinates are also useful when the dimensionality of the problem in physical space can be reduced by a suitable transformation, either because of statistical homogeneity in those directions or because of self-similarity. The number of computational words stored per particle may then be reduced, but at the expense of new terms in the particle evolution equations and the addition of an evolution equation for particle weights. There may also be additional output overhead if it is necessary to transform the statistics of interest to a coordinate system that differs from the computational system.

For the self-similar plane mixing layer treated in Section V, there is no difference in storage requirements between the boundary-layer algorithm and the self-similar algorithm for a given number of particles N; computational times are also comparable. The main advantage of the new algorithm in this case is that the approximations implicit in the boundary-layer approach at low velocity ratios are avoided by working in the self-similar coordinate system. Without the new algorithm, proper treatment of low velocity ratio mixing layers and jets issuing into stagnant surroundings would require a fully two-dimensional scheme.

Acknowledgments

This work was supported in part by Grant CPE-8212661 from the National Science Foundation, Engineering Energetics Program. Computations supporting this research were performed on the Cornell National Supercomputer Facility, which is supported in part by the National Science Foundation and the IBM Corporation.

APPENDIX

In this appendix, transformations from Cartesian to the general orthogonal coordinate systems needed in the treatment of the flows of Section IV are summarized. The notation used is that introduced in Section III. For each transformation, a defining figure is referenced. Then $\mathbf{x} = \mathbf{x}(\bar{\mathbf{x}})$, $h_{(i)}$ (Eq. (51)), a_{ij} (Eq. (54)), $\mu(\bar{\mathbf{x}})$ (Eq. (55)), $\mathbf{C}$ (Eq. (58)), and the Jacobians J_x, J_U, and J (Eqs. (60)–(62)) are reported. Cartesian position and velocity components are denoted by

$$x_1 = x,\ x_2 = y,\ x_3 = z; \qquad U_1 = U_x,\ U_2 = U_y,\ U_3 = U_z. \tag{A1}$$

Scale factors $h_{(i)}$ and components of $\mathbf{C}$ corresponding to the physical velocity components ($\mu = 1$) for cylindrical and spherical coordinates may be found in Appendix 2 of Batchelor [24].

Cylindrical

The cylindrical coordinate system is shown in Fig. 1. The turbulent plane mxing layer becomes self-similar in this coordinate system with statistics of the physical velocity components independent of radial distance r. Position and velocity coordinates are

$$\bar{\mathbf{x}} = \begin{Bmatrix} r \\ \theta \\ z \end{Bmatrix}, \qquad \bar{\mathbf{U}} = \begin{Bmatrix} U_r \\ U_\theta \\ U_z \end{Bmatrix}, \tag{A2}$$

where U_r, U_θ, and U_z are the physical components of the velocity in the r, θ, and z directions, respectively. The transformation from Cartesian coordinates is

$$x = r\cos\theta, \qquad y = r\sin\theta, \qquad z = z, \tag{A3}$$

scale factors $h_{(i)}$ are

$$h_1 = 1, \qquad h_2 = r, \qquad h_3 = 1, \tag{A4}$$

and a_{ij} of Eq. (54) are the components of the matrix

$$\begin{pmatrix} \cos\theta & \sin\theta & 0 \\ -\sin\theta & \cos\theta & 0 \\ 0 & 0 & 1 \end{pmatrix}. \tag{A5}$$

The stretching factor μ and components of $\mathbf{C}$ are

$$\mu = 1, \tag{A6}$$

and

$$C_1 = \frac{U_\theta^2}{r}, \qquad C_2 = -\frac{U_r U_\theta}{r}, \qquad C_3 = 0. \tag{A7}$$

Jacobians of the transformation are

$$J_x = 1/r, \qquad J_U = 1, \qquad J = 1/r. \tag{A8}$$

Modified Cylindrical

The $\mathbf{x} \to \bar{\mathbf{x}}$ transformation is the same as for the cylindrical coordinate system just considered (Eqs. (A3)–(A5)), but now we take $r^{1/2}$ times the physical velocity components as the transformed velocity components (i.e., $\mu = r^{1/2}$). This is appropriate for the turbulent plane jet, where the statistics of $\{r^{1/2}U_r, r^{1/2}U_\theta, r^{1/2}U_z\}$ are independent of r in the self-similar regime. We have, then

$$\bar{\mathbf{x}} = \begin{Bmatrix} r \\ \theta \\ z \end{Bmatrix}, \qquad \bar{\mathbf{U}} = \begin{Bmatrix} r^{1/2}U_r \\ r^{1/2}U_\theta \\ r^{1/2}U_z \end{Bmatrix} = \begin{Bmatrix} U_r' \\ U_\theta' \\ U_z' \end{Bmatrix}. \tag{A9}$$

The stretching factor μ and the components of $\mathbf{C}$ become

$$\mu = r^{1/2}, \tag{A10}$$

and

$$C_1 = \frac{U_\theta'^2 + \frac{1}{2}U_r'^2}{r^{3/2}}, \qquad C_2 = -\frac{U_r' U_\theta'}{2r^{3/2}}, \qquad C_3 = \frac{U_r' U_z'}{2r^{3/2}}. \tag{A11}$$

The Jacobians are

$$J_x = 1/r, \qquad J_U = r^{3/2}, \qquad J = r^{1/2}. \tag{A12}$$

Modified Spherical

For the self-similar axisymmetric jet, we use the spherical coordinate system of Fig. 3 together with the modified velocity components $\{rU_r, rU_\phi, rU_\theta\}$, where U_r, U_ϕ, and U_θ are the physical velocity components in the r, ϕ, and θ directions, respectively ($\mu = r$). Statistics of these modified velocities are independent of r in the self-preserving regime. The transformed coordinates are

$$\bar{\mathbf{x}} = \begin{Bmatrix} r \\ \phi \\ \theta \end{Bmatrix}, \qquad \bar{\mathbf{U}} = \begin{Bmatrix} rU_r \\ rU_\phi \\ rU_\theta \end{Bmatrix} = \begin{Bmatrix} U_r' \\ U_\phi' \\ U_\theta' \end{Bmatrix}. \tag{A13}$$

The transformation in physical space is defined by

$$x = r\cos\phi, \qquad y = r\cos\theta\sin\phi, \qquad z = r\sin\theta\sin\phi, \tag{A14}$$

and

$$h_1 = 1, \qquad h_2 = r, \qquad h_3 = r\sin\phi. \tag{A15}$$

Physical components of a vector transform by the matrix

$$\begin{pmatrix} \cos\phi & \sin\phi\cos\theta & \sin\phi\sin\theta \\ -\sin\phi & \cos\phi\cos\theta & \cos\phi\sin\theta \\ 0 & -\sin\theta & \cos\theta \end{pmatrix}. \tag{A16}$$

The stretching factor and the C_i are

$$\mu = r, \tag{A17}$$

$$C_1 = \frac{U_r'^2 + U_\phi'^2 + U_\theta'^2}{r^2}, \qquad C_2 = \frac{U_\theta'^2}{r^2\tan\phi}, \qquad C_3 = -\frac{U_\phi' U_\theta'}{r^2\tan\phi}, \tag{A18}$$

and the Jacobians are

$$J_x = 1/(r^2\sin\phi), \qquad J_U = r^3, \qquad J = r/\sin\phi. \tag{A19}$$

REFERENCES

1. T. S. LUNDGREN, *Phys. Fluids* **10**, 969 (1967).
2. T. S. LUNDGREN, *Phys. Fluids* **12**, 485 (1969).
3. C. DOPAZO AND E. E. O'BRIEN, *Acta Astronaut.* **1**, 1239 (1974).
4. J. JANICKA, W. KOLBE, AND W. KOLLMANN, *J. Non-equilib. Thermodyn.* **4**, 47 (1978).
5. S. B. POPE, *Phys. Fluids* **24**, 588 (1981).
6. S. B. POPE, *Turbulent Shear Flows 3*, edited by L. J. S. Bradbury, F. Durst, B. E. Launder, F. W. Schmidt, and J. H. Whitelaw (Springer-Verlag, Berlin, 1983), p. 113.
7. S. B. POPE, *AIAA J.* **22**, 896 (1984).
8. M. S. ANAND AND S. B. POPE, *Turbulent Shear Flows 4*, edited by L. J. S. Bradbury, F. Durst, B. E. Launder, F. W. Schmidt, and J. H. Whitelaw (Springer-Verlag, Berlin, 1985), p. 46.
9. S. B. POPE AND M. S. ANAND, *Twentieth Symposium (International) on Combustion*, (The Combustion Institute, Pittsburgh, 1984), p. 403.
10. D. C. HAWORTH AND S. B. POPE, *Fifth Symposium on Turbulent Shear Flows*, edited by L. J. S. Bradbury, F. Durst, B. E. Launder, F. W. Schmidt, and J. H. Whitelaw (Cornell University, Ithaca, New York, 1985), p. 3.13.
11. S. B. POPE AND D. C. HAWORTH, *Turbulent Shear Flows 5*, edited by F. Durst, B. E. Launder, J. L. Lumley, F. W. Schmidt, and J. H. Whitelaw (Springer-Verlag, Berlin, 1987), p. 44.
12. S. B. POPE AND S. M. CORREA, in *Twenty-First Symposium (International) on Combustion* (The Combustion Institute, Pittsburgh, 1986), in press.
13. S. B. POPE AND W. K. CHENG, in *Twenty-First Symposium (International) on Combustion* (The Combustion Institute, Pittsburgh, 1986), in press.

14. S. B. POPE, *Prog. Energy Combust. Sci.* **11**, 119 (1985).
15. D. C. HANDSCOMB AND J. M. HAMMERSLEY, *Monte Carlo Methods* (Methuen, New York, 1965).
16. G. DAHLQUIST AND A. BJORCK, *Numerical Methods* (Prentice–Hall, New York, 1974).
17. S. B. POPE, MIT Report EL-80-012, 1980; revised version, *Combust. Sci. Technol.* **25**, 159 (1981).
18. J. L. LUMLEY, *J. Appl. Mech.* **50**, 1097 (1983).
19. S. B. POPE, *Phil. Trans. R. Soc. London A* **291**, 529 (1979).
20. L. ARNOLD, *Stochastic Differential Equations: Theory and Applications* (Wiley, New York, 1974).
21. D. C. HAWORTH AND S. B. POPE, *Phys. Fluids* **29**, 387 (1986).
22. C. DOPAZO, *Phys. Fluids* **18**, 397 (1975).
23. D. C. HAWORTH AND S. B. POPE, *Stochastic Anal. Appl.* **4**, 151 (1986).
24. G. K. BATCHELOR, *An Introduction to Fluid Dynamics* (Cambridge Univ. Press, London, 1967).
25. S. B. POPE AND R. GADH, Cornell University Report FDA-87-2 (submitted for publication).
26. W. RODI, *Studies in Convection*, edited by B. E. Launder (Academic Press, New York, 1975), Vol. 1, p. 79.
27. H.-H. FERNHOLZ, *Turbulence*, edited by P. Bradshaw (Springer-Verlag, Berlin, 1978), p. 45.
28. D. C. HAWORTH AND S. B. POPE, *Phys. Fluids* **30**, 1026 (1987).
29. T. V. NGUYEN AND S. B. POPE, *Combust. Sci. Technol.* **42**, 13 (1984).